Andean Geology 53 (2): 294-317. May, 2026
doi: 10.5027/andgeoV53n2-3836

Andean Geology
www.andeangeology.cl

SPECIAL ISSUE: RESEARCH ON THE SOUTH WEST MARGIN OF GONDWANA

Early Ordovician Aguada de la Perdiz Formation, northern Chile: Stratigraphy, provenance and regional tectonic setting

***Heinrich Bahlburg[1], Christoph Breitkreuz[2]**

[1] *Institut für Geologie und Paläontologie, Universität Münster, Germany. Corrensstrasse 24, 48149 Münster. hbahlburg@uni-muenster.de*

[2] *Institut für Geologie, Bergakademie Freiberg, Germany. Bernhard von Cotta-Strasse 2, 09599 Freiberg. christoph.breitkreuz@extern.tu-freiberg.de*

* *Corresponding author: hbahlburg@uni-muenster.de*

ABSTRACT. The Early Ordovician Aguada de la Perdiz Formation of northern Chile is one of the oldest unmetamorphosed sedimentary units in Chile. Graptolites indicate a late Floian to early Dapingian age of the formation at the Aguada de la Perdiz type locality and small nearby outcrops in Chile. Correlative outcrops on the Argentinian side occur at Huaitiquina, Filo Pircas, Sierra de Guayaos and Lever Mucar. Graptolites are associated with scarce occurrences of brachiopods and conodonts in some outcrops. In the Argentinian Puna the correlative units were assigned to the Coquena Formation. All outcrops consist mainly of volcaniclastic turbidite and ash-rich flow deposits with intercalations of bimodal lavas, volcanic breccias and reworked felsic tuffs. The lithological assemblage reflects deposition in a marine volcaniclastic apron located on the eastern flank of the Famatinian magmatic arc. We propose to collectively group all respective outcrops in the Aguada de la Perdiz Formation thus respecting precedence of its first definition by García *et al.* (1962) because of the common characteristics of the formation on both sides of the international border. New U-Pb detrital zircon ages of a sample (n=124) from the Huaitiquina locality range between 3,530 and 550 Ma and reflect a common polycyclic provenance from older Amazonian sources. The youngest U-Pb zircon age corresponds to the Ediacaran and predates the biostratigraphically defined depositional age by *ca*. 80 Myr. Thus, the synsedimentary Famatinian felsic volcanism, otherwise common in coeval units, is not reflected in the detrital zircon age record at Huaitiquina. The absence of Famatinian ages may indicate that sediment delivery from the Famatinian arc line source bypassed this site and that erosion of the arc had locally dissected the volcanic edifices and had progressed to access the pre-Pampean Neoproterozoic arc basement.

Keywords: Detrital zircon U-Pb geochronology, Ordovician, N-Chile, Stratigraphy, Provenance.

RESUMEN. La Formación Aguada de la Perdiz (Ordovícico Temprano), norte de Chile: Estratigrafía, proveniencia y marco tectónico regional. La Formación Aguada de la Perdiz, del Ordovícico Temprano en el norte de Chile, constituye una de las unidades sedimentarias no metamórficas más antiguas del país. La presencia de graptolitos indica una edad comprendida entre el Floiano tardío y el Dapingiano temprano en la localidad tipo de Aguada de la Perdiz y en pequeños afloramientos próximos en territorio chileno. Afloramientos correlativos en el sector argentino se encuentran en Huaitiquina, Filo Pircas, Sierra de Guayaos y Lever Mucar. En algunos de estos afloramientos, los graptolitos se asocian a registros escasos de braquiópodos y conodontos. En la Puna argentina, las unidades correlativas han sido asignadas a la Formación Coquena. Todos los afloramientos están constituidos principalmente por turbiditas volcanoclásticas y depósitos de flujo ricos en ceniza, intercalados con lavas bimodales, brechas volcánicas y tobas félsicas retrabajadas. Este conjunto litológico refleja la depositación en un abanico submarino volcanoclástico emplazado en el flanco oriental del arco magmático famatiniano. Se propone agrupar colectivamente todos los afloramientos correspondientes bajo la denominación de Formación Aguada de la Perdiz, respetando la precedencia de su definición original por García *et al.* (1962), en virtud de las características comunes que la unidad presenta a ambos lados de la frontera internacional. Nuevas dataciones U-Pb en circones detríticos de una muestra (n=124) proveniente de la localidad de Huaitiquina registran edades comprendidas entre 3.530 y 550 Ma, lo que refleja una procedencia policíclica común a partir de

fuentes amazónicas más antiguas. La edad U-Pb más joven corresponde al Ediacárico y antecede en aproximadamente 80 millones de años a la edad de depositación definida mediante bioestratigrafía. De este modo, el vulcanismo félsico famatiniano sinsedimentario, común en unidades coetáneas, no se encuentra representado en el registro de circones detríticos de Huaitiquina. La ausencia de edades famatinianas podría indicar que el aporte sedimentario procedente del arco famatiniano no alcanzó este sector, y que la erosión del arco había disectado localmente los edificios volcánicos, permitiendo el acceso al basamento neoproterozoico prepampeano.

Palabras clave: Geochronología de zircons detriticos, Ordovicico, Norte de Chile, Estratigrafia, Procedencia.

1. Introduction

The Late Cambrian to Silurian/Early Devonian accretionary Famatinian orogenic cycle (520-410 Ma) is the second cycle of the Terra Australis Orogen, the evolution of which started at *ca*. 650 Ma (Cawood, 2005). The Famatinian orogenic cycle is recorded along the present western margin of South America from ~36° S to the Mérida Andes of northern Venezuela at ~10° N. It is characterized along its entire length by major intrusive bodies formed in calc-alkaline magmatic arcs between 490 and 460 Ma (Rapela *et al.,* 1990, 1998a, 2018; Pankhurst *et al.,* 1998; Weinberg *et al.,* 2018; see review in Ramos, 2018) (Fig. 1). Rocks metamorphosed at variable depths are abundant and outline a strong tectonic segmentation into exposures of different crustal levels (*e.g.,* Willner *et al.,* 1987; Otamendi *et al.,* 2008; Ramos, 2018; Alasino *et al.,* 2024). Unmetamorphosed or only slightly metamorphosed

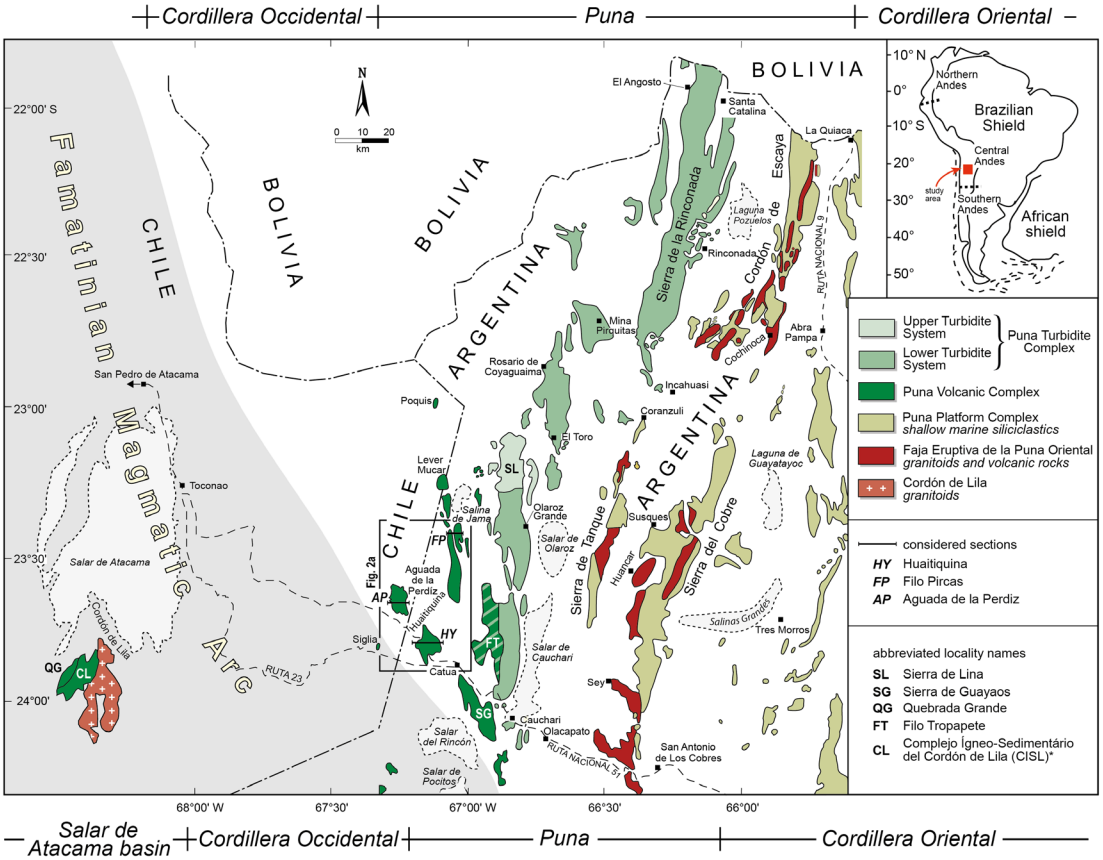

FIG. 1. Outcrop map of Ordovician units in the Puna of northern Chile and northwestern Argentina, and in the Salar de Atacama Basin of northern Chile (modified from Bahlburg, 1990 and Augustsson *et al*., 2015). *sedimentary part.

volcanic rocks are relatively scarce and occur only in those segments where upper crustal levels are exposed. These include relatively widespread occurrences in the Sierra de Famatina (*e.g.,* Armas *et al.,* 2018, 2021; Cisterna and Coira, 2022) and in the Puna of northern Chile and northwestern Argentina (*e.g.,* Schwab, 1973; Breitkreuz, 1986; Coira and Barber, 1989; Coira and Nullo, 1989; Bahlburg, 1990, 1998; Coira *et al.,* 2009a,b) (Fig. 1). Isolated occurrences are in the Cordillera Oriental of southern and central Peru (Haeberlin and Fontbotè, 2002; Bahlburg *et al.,* 2006, 2011) and in the northern Venezuelan Andes (Ramos, 2018).

In this contribution we discuss the main upper crustal non-metamorphic occurrences of volcaniclastic successions in the Puna de Antofagasta of northern Chile and the northern Puna of northwestern Argentina (Figs. 1 and 2). They straddle the international border which impeded cross-border considerations and correlations. We present new detrital zircon U-Pb age data on a sample from the Huaitiquina outcrop on the Argentinian side. We consider the new detrital zircon age data jointly with similar data from the broadly coeval Complejo Ígneo-Sedimentario del Cordón de Lila (CISL; Niemeyer, 1989) (Fig. 1) in the Salar de Atacama basin to the west in order to clarify the regional implications of the new data for their host formations.

2. Stratigraphic framework of Ordovician units in the Puna of northern Chile and northwestern Argentina

The Aguada de la Perdiz Formation was the first recognized stratigraphic unit of Ordovician age in Chile and is located in the Puna de Antofagasta of northern Chile. Together with the Early Ordovician sedimentary rocks of the CISL (Figs. 1 and 3) it is the oldest unmetamorphosed sedimentary unit on continental Chilean territory. Its base and top are unseen. The formation was first described and named by García *et al.* (1962) and was assigned to the Lower

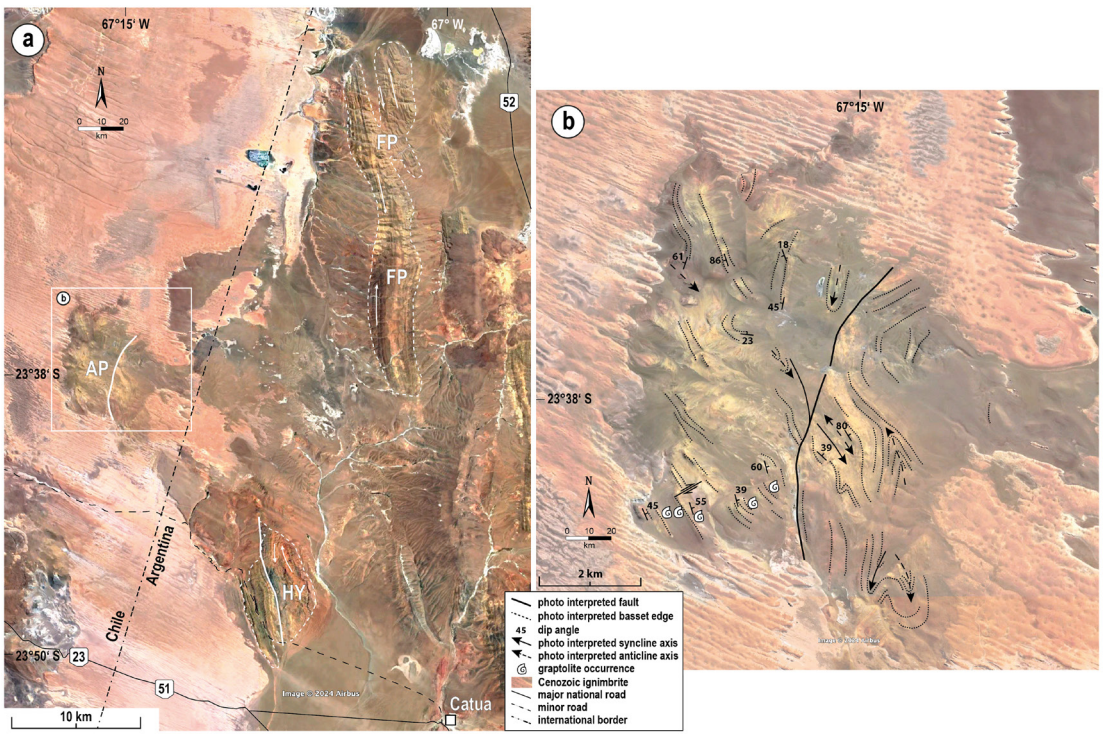

FIG. 2. Google Earth satellite images (2025) of the Aguada de la Perdiz Formation. **A.** Overview of the Aguada de la Perdiz (AP), Huaitiquina (HY) and Filo Pircas (FP) localities. **B.** Interpretation of satellite image photolineations of the Aguada de la Perdiz outcrop, adapted from Breitkreuz (1986). Stars and labels indicate sampling localities, sample 09AA31: Einhorn *et al*. (2015), sample HY19: this contribution.

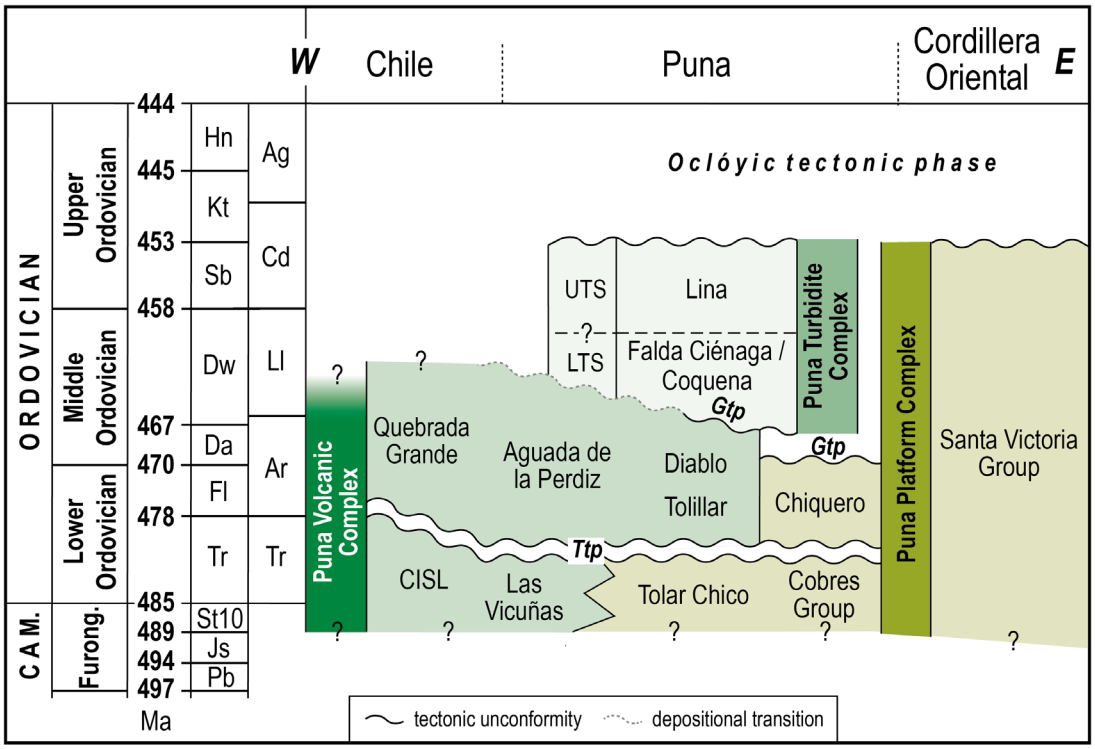

FIG. 3. Uppermost Cambrian and Ordovician stratigraphy and formations of the Puna of northern Chile and northwestern Argentina (compiled and adapted from Schwab, 1973; Breitkreuz, 1986; Aceñolaza and Baldis, 1987; Bahlburg *et al*., 1990; Moya *et al*., 1993; González *et al*., 2007; Brussa *et al*., 2008; Moya, 2015; Toro and Herrera Sánchez, 2019; and J. Maletz, pers. comm., 2022, 2025). ICS chronostratigraphy according to Cohen *et al*. (2013, updated). **Pb**: Paibian; **Js**: Jiangshanian; **ST10**: unnamed Stage 10; **Tr:** Tremadocian; **Fl**: Floian; **Da**: Dapingian; **Dw**: Darriwilian; **Sb**: Sandbian; **Kt**: Katian; **Hn**: Hirnantian; **Ar**: Arenig; **Ll**: Llanvirn; **Cd**: Caradoc; **Ag**: Ashgill; **Ttp**: Tumbaya tectonic phase; **Gtp**: Guandacol tectonic phase; **CISL**: Complejo Ígneo-Sedimentario del Cordón de Lila; **LTS**: Lower Turbibidite System; **UTS**: Upper Turbidite System.

Ordovician Arenig Series (now Floian-Dapingian; Fig. 3) on the basis of graptolite finds. Additional graptolite fauna found at related outcrops in the vicinity (Poquis, Lever Mucar; Figs. 1 and 2A) led Pérez (1983) to group all these occurrences in the Aguada de la Perdiz Formation with a corresponding age range encompassing the Arenig and Llanvirn (now Floian to Darriwilian; Fig. 3; Table 1).

On the Argentinian side it was Schwab (1973) who first found upper Arenig (now Dapingian; Fig. 3; Table 1) graptolites at Filo Pircas in a succession of greywackes and shales with diabase intercalations (Figs. 1 and 2). He was the first who in this context suspected a volcanic origin also for the cherts ('pedernal'; García *et al.,* 1962) of the upper Aguada de la Perdiz Formation and correlated his graptolite finds with those on the Chilean side. This was later substantiated with correlative finds in volcaniclastic strata in the Sierra de Guayaos near Catua (Aceñolaza and Durand, 1974; Coira *et al.,* 1987) (Figs. 1 and 2A; Table 1) and, together with conodonts of the same age, at Huaitiquina (Monteros *et al.,* 1996; Toro *et al.,* 2019, 2020) (Table 1). Following Schwab (1973), the respective rocks on the Argentinian side were assigned to the Coquena Formation of Dapingian to Darriwilian age (*e.g.,* Monteros *et al.,* 1996; Toro *et al.,* 2019, 2020) (Fig. 3; Table 1). Ordovician brachiopods confirming the age assignments indicated by the graptolites were found in similar rocks at several localities south of the study area (*e.g.,* Benedetto, 2001, 2003). Bahlburg *et al.* (1990) presented additional graptolite data, further constraining the stratigraphic relationships between the Aguada de la Perdiz Formation and equivalents and the partly coeval and younger Ordovician turbidite units farther east in the Argentinian Puna (Figs. 1 and 3).

TABLE 1. GRAPTOLITE FAUNAS AND STRATIGRAPHIC AGES OF DIFFERENT OUTCROPS OF THE AGUADA DE LA PERDIZ FORMATION.

Outcrop*	Fauna	Stratigraphic age**	British series
Aguada de la Perdiz	*Tetragraptus approximatus* *Didymograptus (Didymograptellus)* cf. *bifidus* *Didymograptus* cf. *Didymograptellus bifidus* *Didymograptus* sp. *Tetragraptus quadribrachiatus* *Didymograptus constrictus* *Didymograptus ensjoensis* *Expansograptus urbanus* *Expansograptus* cf. *suecicus* *Expansograptus* cf. *constrictus* *Tetragraptus* cf. *serra* *Tetragraptus (Etagraptus)* cf. *harti* cf. *Phyllograptus* cf. *Expansograptus* cf. *Tetragraptus serra* cf. *Tetragraptus amii*	*Tetragraptus approximatus*, **early Floian (Fl1)** *Didymograptellus bifidus* biozone, **late Floian (Fl3)**	early to middle Arenig
Huaitiquina	*Azygograptus lapworthi* *Isograptus* sp. *Pseudotrigonograptus minor* *Xiphograptus lofulensis* *Dichograptus octobrachiatus* *Tetragraptus bigsbyi* *Xiphograptus* sp. **Conodonts** *Baltoniodus* cf. *B. navis* *Gothodus* cf. *G. costulatus* *Trapezognathus quadrangulum*	*Azygograptus lapworthi* biozone, **early Dapingian (Dp1)** *Isograptus* sp., **middle Dapingian (Dp2)** *Baltoniodus navis* biozone***, **middle Dapingian (Dp2)**	middle to late Arenig
Filo Pircas (Filo Tropapete; Schwab, 1973)	*Didymograptus* cf. *hirundo* *Didymograptus* cf. *gracilis* *Glossograptus* cf. *hincksii mut. bispinatus* *Expansograptus* sp.	**late Floian (Fl3)-early Dapingian (Dp1)**	middle to late Arenig

Table 1 continued.

Outcrop*	Fauna	Stratigraphic age**	British series
Sierra de Guayaos/Catua	*Tetragraptus quadribrachiatus catuaensis* *Dichograptus octobrachiatus* *Tetragraptus quadribrachiatus*	**early Darriwilian (Da1)**	late Arenig
Poquis	*Cryptograptus* (?) *antennarius* *Glossograptus* sp. *Isograptus* sp. *Didymograptus* sp. *Dicellograptus* sp.	**Darriwilian (Dw)**	Llanvirn
Lever Mucar	*Didymograptus sagitticaulis* *Didymograptus compressus*	**Darriwilian (Dw)**	Llanvirn
Quebrada Grande Formation, Cordón de Lila	*Tetragraptus* sp. *Cryptograptus*? sp. **Brachiopods** *Paralenorthis* sp. *Monorthis transversa* *Mollesella?* sp.	**Darriwilian (Dw)**	late Arenig to early Llanvirn

* for outcrops see figure 1.
** age assignment of graptolite biozones after Goldman *et al.* (2023).
*** age assignment of conodont biozone after Toro *et al.* (2020).
compiled from Fuenzalida (1957), García *et al*. (1962), Schwab (1973), Aceñolaza and Durand (1975), Pérez (1983), Breitkreuz (1986), Coira and Nullo (1989), Bahlburg *et al.* (1990), Gutierrez-Marco *et al*. (1996), Monteros *et al*. (1996), Benedetto *et al.* (2008), Toro *et al.* (2019, 2020), and J. Maletz (pers. comm., 2022, 2025). Conodonts at Huaitiquina from Toro *et al.* (2020). Graptolites and brachiopods of the Quebrada Grande Formation from González *et al.* (2007). For global stratigraphic stages see figure 3.

Until recently, the Ordovician stratigraphic schemes of the Chilean and Argentinian Puna were kept almost completely separate. It was noted that the lower Coquena Formation (Fig. 3) contained volcanic and volcaniclastic rocks which were broadly coeval with the Aguada de la Perdiz Formation directly on the other side of the border in Chile (Schwab, 1973) but the schemes were not unified. To simplify matters, Bahlburg *et al.* (1990) combined all of the volcanic and volcaniclastic units of Floian to Darriwilian age of the Chilean and Argentinian Puna under the informal name Volcanosedimentary Successions of the Puna, for which we now suggest the name Aguada de la Perdiz Formation because it has precedence. As the respective volcanic record had, however, started already in the Tremadocian Las Vicuñas Formation (Moya *et al.,* 1993), we combine here all Lower and Middle Ordovician volcanic and volcaniclastic units in the Puna Volcanic Complex, including the redefined Aguada de la Perdiz Formation (Fig. 3).

3. The original Aguada de la Perdiz Formation

Fuenzalida (1957) was the first to report the presence of Ordovician sedimentary rocks in the Puna of Antofagasta of northern Chile bearing the graptolite *Didymograptus sagitticaulis* at the Lever Mucar locality (Fig. 1; Table 1). The Aguada de la Perdiz Formation (Figs. 1-3) was established by García *et al.* (1962) who described a ~2,000 m thick siliciclastic succession divided into two parts, a lower member of quartz-rich sandstones yielding the graptolites *Didymograptus* sp., *Tetragraptus quadribrachiatus* and *Tetragraptus approximatus*, and an upper member consisting mainly of cherts ('pedernal'; Fig. 3; Table 1). The formation is exposed at altitudes of 4,400-4,600 m a.s.l. at the eastern margin of the volcanoes of the Cordillera Occidental (Figs. 1 and 2). Marinovic (1979) and Pérez and Davidson (1982) added finds of *Glossograptus* sp. and *Isograptus* sp., among others (Table 1), at the isolated Poquis locality north of Aguada de la Perdiz (Fig. 1) and recognized the sedimentary rocks as a succession of turbidites. The summary of available graptolite data by Pérez (1983) was extended by Breitkreuz (1986) who reported a rather diverse graptolite fauna including *Didymograptus bifidus* (Table 1) which helped to place the Aguada de la Perdiz outcrop in the mid-Floian *bifidus* zone of the Lower Ordovician (Table 1). The combination of biostratigraphic data from the Chilean Aguada de la Perdiz, Poquis and Lever Mucar localities indicates a stratigraphic range of the Early and Middle Ordovician units from the mid-Floian into the Darriwilian (Arenig-Llanvirn of the British Series; Fig. 3, Table 1).

3.1. Depositional facies

Breitkreuz (1986) was the first to observe the volcanic nature of the Aguada de la Perdiz Formation at its type locality (Figs. 1, 2, 4, and 5A). He upheld the original division of the formation by García *et al.* (1962) into two members (Fig. 4). The lower coarse-grained member consists of a ~1,500 m thick succession of red to multi-colored (Figs. 4 and 5B) volcaniclastic strata including felsic volcaniclastic debris flow deposits (Fig. 5B-D). It is overlain by the ~1200 m thick upper member of silicified, fine-grained and thin-bedded tuffs, reworked tuffs and mass flow deposits with colors ranging from greyish-black to brownish-yellow (Figs. 4, 5A, and 5E).

As summarized from Breitkreuz (1986) and Breitkreuz *et al.* (1989), the coarse-grained volcaniclastic rocks of the lower member consist of sandy-conglomeratic beds up to one meter thick, interspersed with thin, fine-sandy to pelitic, locally fossiliferous layers (Fig. 2B). Thick monomict and polymict breccia tuffs, reaching up to 15 m, are occasionally intercalated (Fig. 5B, C). The sandy-conglomeratic beds maintain a consistent lateral thickness and exhibit normal and coarse-tail grading (Fig. 5B).

According to Breitkeuz (1986) and Breitkreuz *et al.* (1989) volcaniclastic sandstones display compaction structures including pressure solution and crystal deformation parallel to bedding planes alongside partial carbonate replacement. The matrix consists of fine-grained chert, with former glass shard outlines visible under the microscope in unpolarized light. The framework components, in decreasing abundance, include resorption-embayed quartz, sanidine, variably sericitized andesine/labradorite, devitrified pumice fragments. Fibrous cherts, and accessory minerals such as biotite (partly chloritized), opaques, and zircon complete the picture. Non-volcanic quartzite rock fragments occur in the conglomerates.

Breccia tuffs are intercalated in the lower member. They either consist of rhyolitic components including non-graded ash layers, or siliceous tuff clasts, reaching up to one meter in size, along with

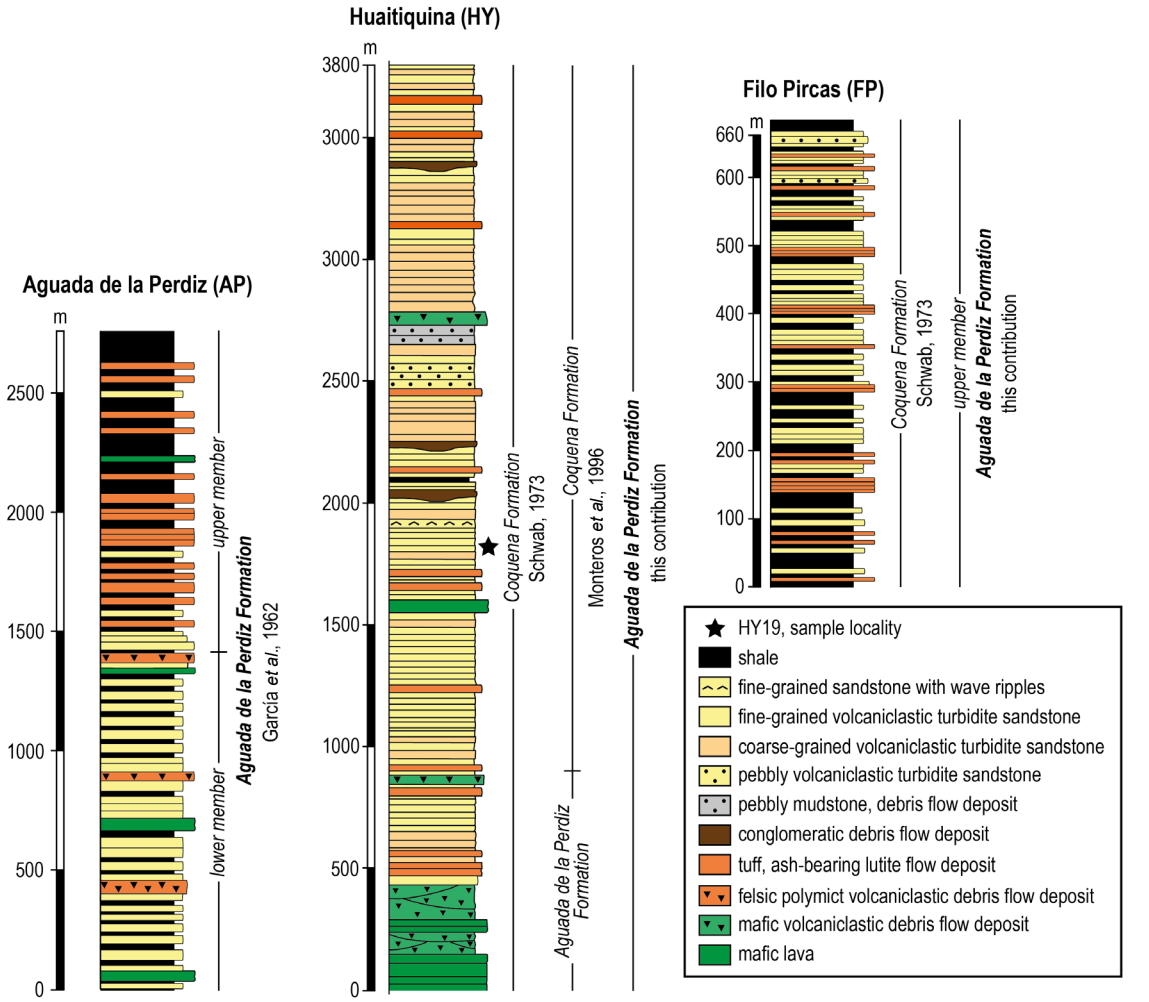

FIG. 4. Schematic lithostratigraphic sections of the Aguada de la Perdiz Formation at the type locality (AP), and at Huaitiquina (HY) and Filo Pircas (FP). AP redrawn and modified from Breitkreuz (1986) and Bahlburg *et al*. (1990); HY redrawn and modified from Bahlburg (1990) and Monteros *et al*. (1996); FP redrawn from Bahlburg *et al*. (1990). The asterisk in HY marks the origin of detrital zircon sample HY19 shown in figure 7.

plastically deformed, laminated tuff rafts suspended in a trachytic tuff groundmass (Fig. 5C). Component size decreases rapidly toward the top of the breccia tuffs.

The composition of the breccia matrix includes basaltic hydroclastic fragments with vesicles and perlitic cracks suggesting proximal subaquatic magmatic activity. They occur jointly with aphanitic to intersertal volcanic fragments and siliceous tuff clasts compositionally similar to the larger breccia components. Similar sedimentary bodies have been described by White and Busby-Spera (1987) as deposits of 'short-distance, weakly turbulent, high-concentration sediment flows.'

The coarse-grained volcaniclastic deposits of the lower section of the formation lack evidence of a hot regime of transport and sedimentation including the absence of any indication of welding and fusion of particles. The succession is best characterized as a thick stack of volcaniclastic turbidity current and debris flow deposits (Cas and Wright, 1987).

The transition from the lower coarse-grained to the upper fine-grained member is marked by a ~10 m thick fining- and thinning-upward sequence. The upper member consists of 20-50 cm thick tuffs and reworked tuffs, the latter characterized by fine cross beds, parallel and convolute lamination, and

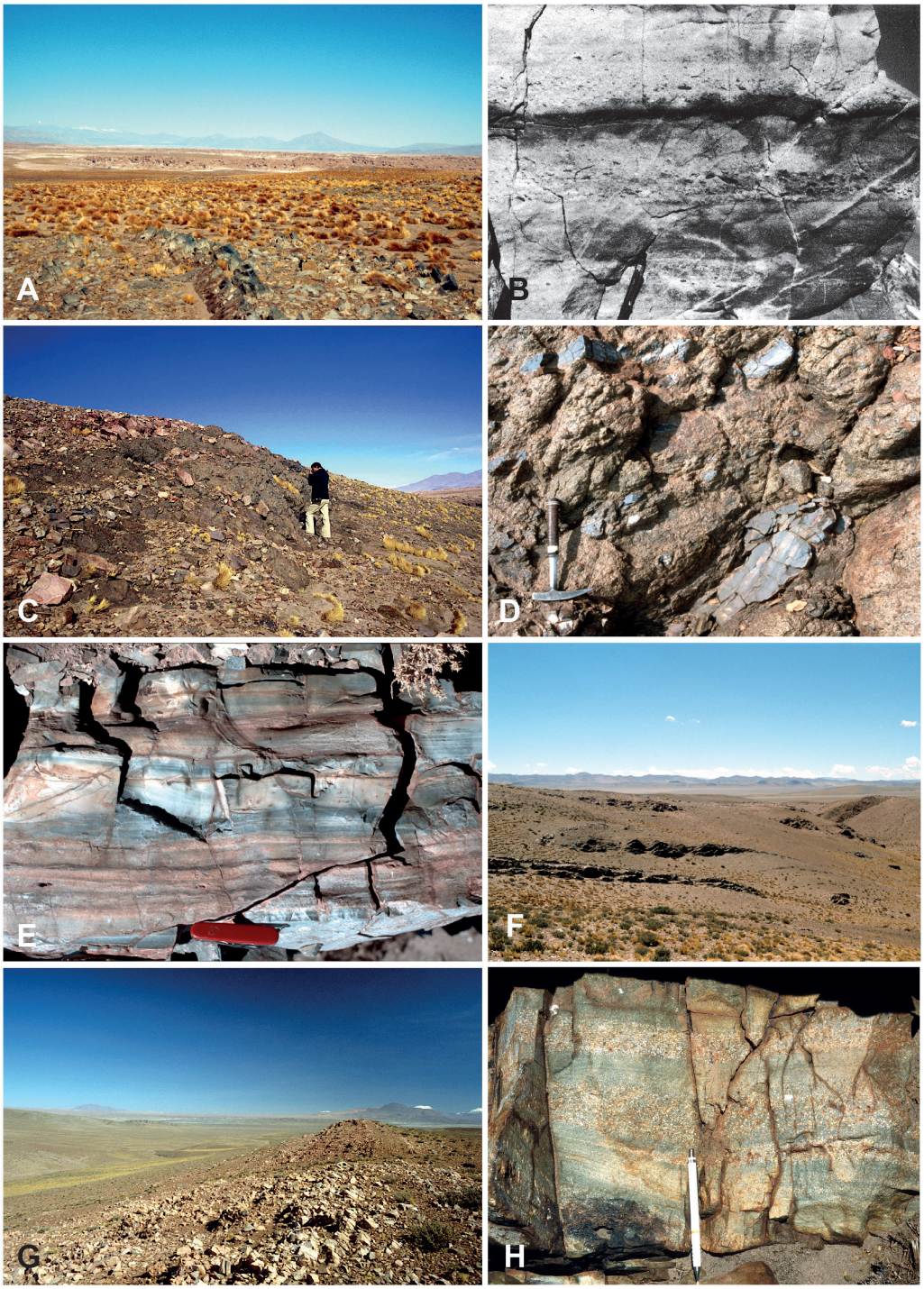

FIG. 5. Outcrop pictures of the Aguada de la Perdiz Formation at the type locality (A-E) and at the Filo Pircas section (F-H). **A.** Outcrop overview with thin-bedded ash-bearing flow deposits of the upper member in foreground and Cenozoic ignimbrite cover in the middleground. **B.** Submarine rhythmic coarse-tail graded volcaniclastic turbidites, upper member (from Breitkreuz, 1986). **C-D.** Outcrop view and detail of lower member felsic volcaniclastic debris flow deposit with rafts of fine-grained ash-bearing flow deposits. **E.** Detail of upper member ash-bearing flow deposit showing cross-bedding. **F.** Outcrop overview. **G.** Thin-bedded ash-bearing flow deposits. **H.** Graded volcaniclastic turbidites (from Bahlburg, 1990).

cut-and-fill structures deposited from ash-bearing flows (White and Busby-Spera, 1987) (Figs. 4 and 5E). Less silicified, thinly bedded siltstone and claystone intercalations locally contain graptolites and phyllocarids (Breitkreuz, 1986).

Thin-section analysis of the tuffs reveals a fine-grained, devitrified groundmass with remnants of former glass shards. Small amounts of quartz, feldspar, biotite, and chert fragments are arranged in layers within this matrix. Patchy carbonatization is also observed in some areas.

A few meter-thick mafic lavas occur in the formation. In the lower member they consist of aphanitic to intersertal-textured rocks, primarily composed of variably altered plagioclase and augite. The mafic lava in the upper part of the fine-grained section is an altered basalt containing chalcedony- and carbonate-filled amygdales, along with some feldspar phenocrysts.

3.2. Depositional environment

The depositional environment is interpreted as marine because of the presence of graptolite-bearing strata (Pérez, 1983; Breitkreuz, 1986; Monteros *et al.,* 1996). The preservation and abundance of turbidites indicates that the depositional site was below storm wave base and at the base of some considerable relief conducive to the formation of turbidity currents and debris flows.

The characteristics of lithology and facies suggest that the Aguada de la Perdiz Formation represents a submarine volcaniclastic apron (White and Busby-Spera, 1987) of a mid-Floian (Fl3; Table 1) possibly subaerial chain of bimodal but predominantly felsic volcanoes (Breitkreuz, 1986; Bahlburg, 1990). Periodically, this apron experienced subaqueous lava extrusions indicating activity of nearby mafic vents. While sporadic proximal felsic volcanic activity is indicated by a few massive rhyolitic breccia tuffs, the dominance of turbidity current over debris flow deposits suggests that the formation developed distally from the primary source of volcanic debris. The extent to which air fall contributed to the deposition of the volcaniclastic strata is unknown. Low-density turbidity currents and/or dilute, slow-moving ash-bearing flows were responsible for forming submarine, rhythmic, fine-grained tuff successions typical of the upper member of the Aguada de la Perdiz Formation (Figs. 4, 5A, and 5E).

4. Correlative units in the neighbouring Puna of northwestern Argentina

4.1. Huaitiquina

The Aguada de la Perdiz Formation at the Huaitiquina locality (Figs. 1 and 2) is exposed at altitudes of 4,200-4,400 m a.s.l. The base of the section is formed by the westernmost NNW-SSE striking anticline in the eastern part of the outcrop area. Along a fault in the Río Huaitiquina valley there is a repetition of strata, which is accounted for in figure 4. The top of the section is covered by Cenozoic rocks.

Schwab (1973) characterized the strata of the Río Huaitiquina area as conglomeratic greywackes with intercalations of diabasic lavas and tuffs. Méndez *et al.* (1979) documented a 920 m thick section of intercalated clastic rocks and andesites which presumably represent the lower part of the exposed section (Figs. 4 and 6A). Coira and Barber (1987) divided the succession into five parts which, in their interpretation, mirror the evolution from andesitic to explosive siliceous and submarine arc volcanism, the latter of which is succeeded by epiclastic sedimentary rocks (Fig. 6B). The described section is 1,100 m thick.

In detail the complete section begins with a ~500 m thick sequence of strongly jointed subaqueous vesicular basalt, basaltic andesite and andesite lavas and associated hydroclastic breccias (Fig. 6C, D). They are intercalated with mostly coarse-grained monomict mafic debris flow deposits with minor grading at the top and are overlain by polymict and felsic partly brecciated debris flow deposits (Fig. 6E) some of which contain rafts of deformed laminated siliceous tuffs up to one meter in diameter similar to the ones found at the Aguada de la Perdiz locality (cf. Fig. 5D). These give way to coarse and fine-grained volcaniclastic turbidites (Fig. 6F). Well sorted sandstones with 2-3 cm high symmetric wave ripples are intercalated at the top of this lower volcanic section (Figs. 4 and 6G).

The middle and upper part of the ~3,300 m thick succession consists of volcaniclastic fine- to coarse-grained and partly graded sandy turbidites. Further basalt lavas are intercalated occasionally in the upper section and up to 40 m thick packages of 20-50 cm thick siliceous, laminated tuffs are common (cf. Fig. 5E). Some of the tuffs have a weakly erosive base. Massive and graded sandstones and pebbly sandstones are deposits from turbidity currents.

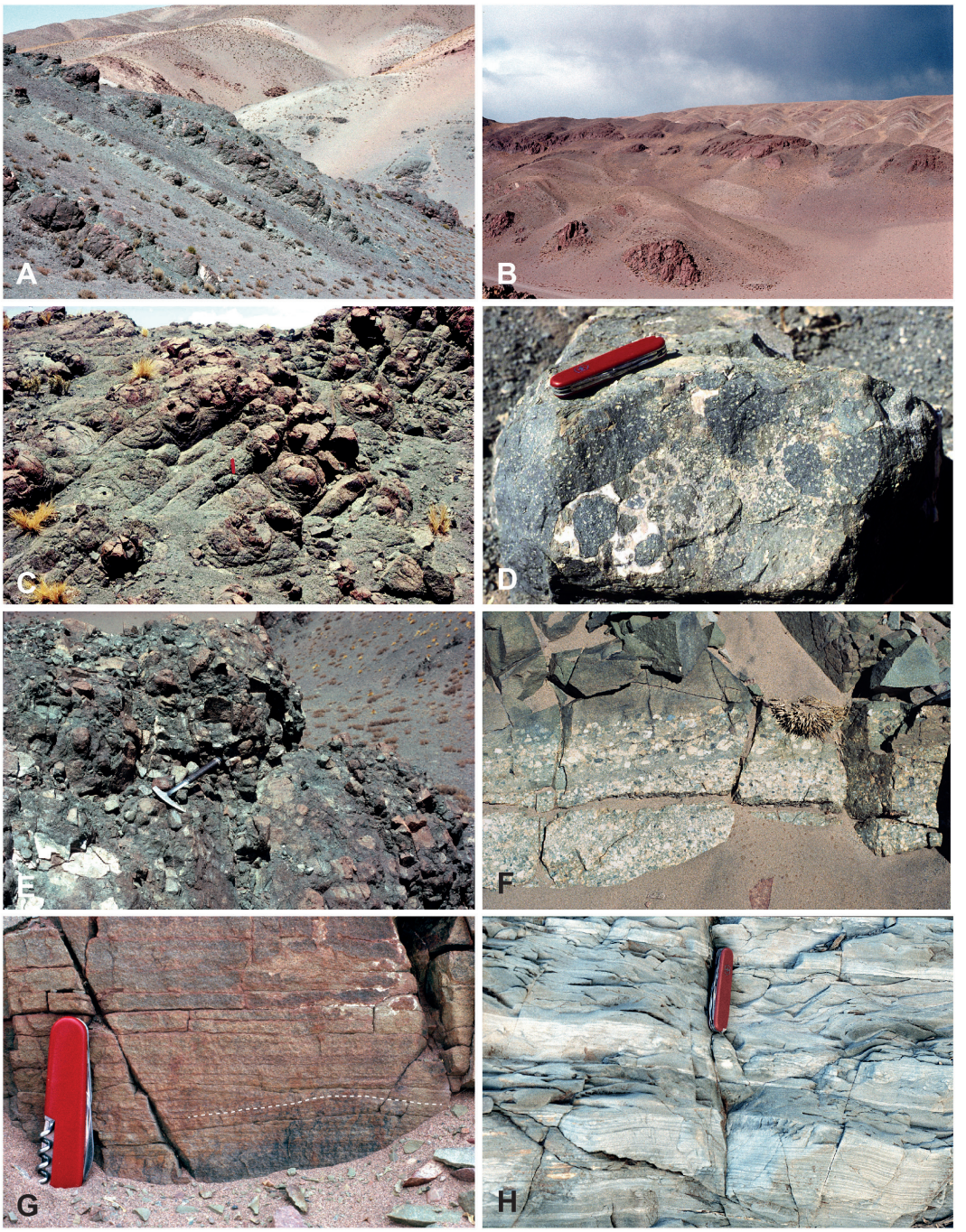

FIG. 6. Outcrop pictures of the Aguada de la Perdiz Formation at the Hyuaitiquina locality. **A.** Overview of lower part of the section with alternating dark mafic lavas and debris flow deposits in the foreground, and red to light colored volcaniclastic turbidite sandstones and debris flow deposits in the background. **B.** Overview of upper part of the section with predominant volcaniclastic turbidite sandstones and debris flow deposits. **C.** Jointed basaltic-andesite lavas. **D.** Mafic hydroclastic breccia. **E.** Mafic volcaniclastic debris flow deposit (from Bahlburg, 1990). **F.** Pebbly volcaniclastic turbidite overlain by coarse-grained volcaniclastic turbidite sandstone. **G.** Sandstone with symmetrical wave ripples (dashed white line). **H.** Alternations of laminated and massive fine-grained turbidites; bed with pocket knife shows ball and pillow dewatering structures.

4.2. Filo Pircas

The 660 m thick Filo Pircas section (FP; Figs. 1, 2, and 4) is exposed at an altitude of 4,200-4,400 m a.s.l., between a syncline in the west and an anticline in the east (Bahlburg, 1990). 3-20 m thick successions of fine-grained and thin-bedded (10-50 cm) volcaniclastic turbidites (Fig. 5F, H) alternate with 5-20 m thick successions of thin (5-15 cm) laminated tuffs which frequently have an erosional base (Fig. 5G, H). Thickness and abundance of the tuffs decrease up section.

The outcrop at Lever Mucar (Fig. 1) represents an along-strike continuation of the Filo Pircas section and appears to contain more epiclastic sandstones and shales in the northern reaches of the outcrop (Coira and Nullo, 1989).

4.3. Nature of magmatism in the Aguada de la Perdiz Formation

Mafic volcanic arc lavas are most abundant in the lower member of the Aguada de la Perdiz Formation and give way to more felsic volcanism up-section (Schwab, 1973; Breitkreuz *et al.,* 1989; Coira and Barber, 1989; Bahlburg, 1990) (Fig. 4). The geochemical characteristics identify both mafic and felsic volcanic rocks as calc-alkaline and related to the activity of the Ordovician Famatinian volcanic arc (Faja Eruptiva de la Puna Occidental; Palma *et al.,* 1986) above an east-dipping subduction zone (present coordinates) along the evolving Famatinian accretionary orogen (Coira *et al.,* 1982, 1999, 2009b; Coira and Barber, 1987, 1989; Breitkreuz *et al.,* 1989; Bahlburg, 1990, 1998; Niemeyer *et al.,* 2018; Ramos, 2018).

4.4. Depositional facies of the Huaitiquina and Filo Pircas localities and biostratigraphic correlation to the Aguada de la Perdiz locality

Submarine basalts and andesites and associated debris flow deposits characterize the lower 500 m of the Huaitiquina section. This mafic magmatism is associated with felsic tuffs which occur as extensive layers or reworked as rafts in the debris flow deposits. Lithologically related tuffs which lack the erosive base may have been connected to submarine effusions and may have been deposited from suspension (White and Busby-Spera, 1987). Similar to the Aguada de la Perdiz Formation at the type locality, the partly cross-bedded tuffs are interpreted to have a subaerial origin and were subsequently deposited in a marine environment by dilute slow-moving ash-rich flows.

Coira and Barber (1987) found thin stromatolites in the lower part of their section in the Huaitiquina area. The combination of (i) the stromatolites, (ii) wave rippled sandstones, and (iii) the sparse graptolite and conodont fauna (Monteros *et al.,* 1996; Toro *et al.,* 2020) (Table 1) indicates shallow marine conditions during deposition of the lower part of the Huaitiquina section. Volcaniclastic turbidites dominate up-section and point to an increase in water depth and subsidence of the marine depositional site through time.

The deposits of the Filo Pircas section document the increasing abundance up-section of volcaniclastic, predominantly fine sand turbidites and ash-rich flow deposits commonly with an erosional base (Fig. 4; Table 1). The Filo Pircas section is rather similar to the upper member of the Aguada de la Perdiz Formation at the type locality and may be a biostratigraphic equivalent to this member in the late Floian and lower Dapingian (Fig. 4; Table 1). It may also represent an equivalent of the finer grained upper part of the Huaitiquina section (Fig. 4; Table 1).

Overall, the depositional environment of the Aguada de la Perdiz Formation is that of a volcaniclastic apron connected to the bi-modal Famatinian volcanic arc source. The arc was located to the west between the discussed outcrops and the CISL in the Salar de Atacama basin. The volcaniclastic Aguada de la Perdiz Formation formed on the back-arc flank (Breitkreuz, 1986; Palma *et al.,* 1986; Bahlburg, 1990; Niemeyer *et al.,* 2018) (Fig. 1). The facies differences between the Aguada de la Perdiz and Huaitiquina localities are likely due to a variable local input along the Famatinian magmatic arc source.

East of the discussed outcrops, at Filo Tropapete (Schwab, 1973) (Fig. 1), the strata of the Aguada de la Perdiz Formation pass gradually into the turbidite successions of the Lower Turbidite System (Coquena Formation; Schwab, 1973; Bahlburg, 1990) (Fig. 3). The Huaitiquina site records a marked deepening from shallow water depth with stromatolites to deeper subtidal depths at rates of up to 1,100 m/Myr (Bahlburg, 1990), allowing the deposition of thick successions of turbidites. In view also of the accumulation of the Puna Turbidite Complex (Fig. 3) east of the Aguada de la Perdiz Formation, a deepening of the basin in eastward direction is inferred (Bahlburg, 1990).

The lithological development of the Filo Pircas section and the Filo Tropapete, and by correlation also of the upper sections at Aguada de la Perdiz and Huaitiquina, is interpreted to be the result of the waning of volcanic activity and the erosion of the volcanic edifices farther west during the upper Dapingian and the lower Darriwilian (Bahlburg, 1990) (Fig. 3).

5. New detrital zircon U-Pb ages of the Aguada de la Perdiz Formation

Einhorn *et al.* (2015) presented a few reliable detrital zircon ages (n=9) obtained from a detrital sedimentary sample of the Aguada de la Perdiz Formation at its type locality. These ages range from *ca.* 476 to 465 Ma and include a youngest population with a weighted mean age of 465±4 Ma (lower Darriwilian; n=5) and a youngest zircon age of 453±12 Ma. Both are commensurate with the lower Darriwilian biostratigraphic age of the formation. In order to further constrain and broaden the age and provenance information on the Aguada de la Perdiz Formation we dated detrital zircon in a single sandstone sample (HY19) from the Huaitiquina locality.

5.1. Methods

Zircons were analysed for U-Pb geochronology by LA-ICP-MS at the Institute for Mineralogy at the University of Münster using a ThermoFisher Element2 mass spectrometer coupled to a Photon Machines Analyte G2 Excimer laser. The specific procedural details are reported in a large number of studies including Kooijman *et al.* (2012) and Bahlburg *et al.* (2016, 2020).

The zircons consist predominantly of euhedral, elongate or short prismatic as well as subrounded to rounded grains usually less than 150 μm in length. The cathodoluminescence images show oscillatory or sector zoning interpreted as of magmatic origin; unzoned grains or those with irregular and round zoning are considered to be of metamorphic origin (Vavra *et al.,* 1999). Zircon rims were preferentially analyzed to date the last growth stage of each zircon.

We uniformly apply a concordance filter of 90 and 101% to all our data (see Supplementary Table 1) with 124 U-Pb ages fulfilling this criterion. 120 age dates have errors between 1 and 5%, averaging 2.3%. For zircons older than 1.5 Ga the $^{207}Pb/^{206}Pb$ ages are used and for those younger the $^{206}Pb/^{238}U$ ages are preferred. We follow Spencer *et al.* (2016) who evaluated the error dimensions of 38,000 published zircon ages and recommended the crossover point from $^{207}Pb/^{206}Pb$ ages to $^{206}Pb/^{238}U$ ages be placed at 1.5 Ga. Kernel Density Estimates (KDE) were calculated with the *provenance* software package (Vermeesch *et al.,* 2016).

5.2. Results

The detrital zircon U-Pb ages of sample HY19 from the middle part of the Huaitiquina section (Fig. 4) range between 3,529±31 Ma and 552±9 Ma (Supplementary Table 1). Major abundance maxima are at *ca*. 1,550, 1480, and 1060 Ma, with minor ones at *ca*. 1,760 and 650 Ma (Fig. 7). Multiple studies have demonstrated an Amazonian and proto-Andean origin of the detritus constituting the (Early) Paleozoic sedimentary rocks of the Andean region (*e.g.,* Willner *et al.,* 2008; Bahlburg *et al.,* 2009, 2011, 2025; Augustsson *et al.,* 2015; Einhorn *et al.,* 2015; Pankhurst *et al.,* 2016). The listed maxima can be apportioned to the major orogenic and tectonic cycles reflecting the crustal evolution of Amazonia since the beginning of the Paleoproterozoic with individual zircon ages extending back to the Paleoarchean (*e.g.,* Cawood, 2005; Cordani and Teixeira, 2007; Pepper *et al.,* 2016; Bahlburg *et al.,* 2025) (Fig. 7).

In decreasing order of abundance, the Huaitiquina sample (Fig. 7) includes 27% of grains linking back to the Rondonia-San Ignacio orogenic cycle (1,550-1,200 Ma), 26% to the Sunsás cycle (1,200-1,000 Ma), 21% to the Río Negro-Juruena cycle (1,800-1,550 Ma), 9% to the phase of Neoproterozoic rifting connected to the breakup of Rodinia (1,000-650 Ma; Cawood *et al.,* 2016; Bahlburg *et al.,* 2020), 6% to the Central Amazonian Province (>2,300 Ma), 5% to the Ventuari-Tapajos cycle (2,000-1,800 Ma), and 3% each to the Maroni-Itacaiunas (2,300-2,000 Ma) and the Olmos-Pampean cycles (650-520 Ma; Cordani and Teixeira, 2007; Bahlburg *et al.,* 2025) (Fig. 7). There are no syndepositional Ordovician detrital zircon ages. The age spectrum is thus dominated by Paleo- and Mesoproterozoic ages recording the evolution of the Terra Amazonica Orogen (Bahlburg *et al.,* 2025) (Fig. 7).

The youngest age peak is represented by two grains giving an average mean age of 652 Ma (Fig. 7).

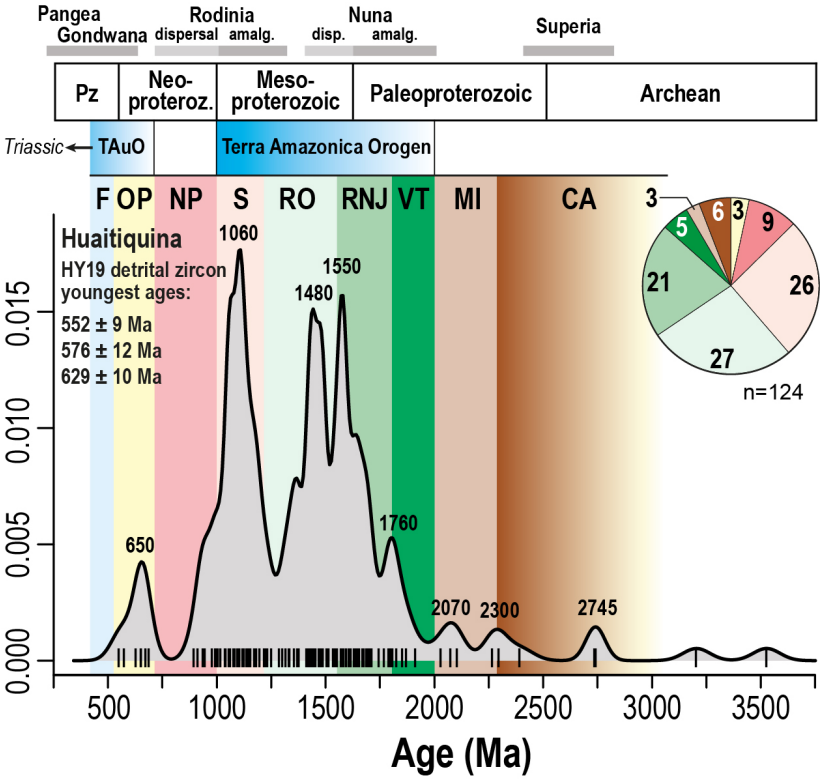

FIG. 7. Kernel Density Estimates (KDE, bandwidth 25) of zircon U-Pb ages of detrital zircon in the lower Ordovician Aguada de la Perdiz Formation at Huaitiquina (HY19). Abbreviations of orogens and orogenic and tectonic cycles according to Bahlburg *et al*. (2025). **TAuO**: Terra Australis Orogen. **CA**: Central Amazonian. **F**: Famatinian. **MI**: Maroni-Itacaiunas (Transamazonian). **NP**: Neoproterozoic rifting. **OP**: Olmos-Pampean. **RNJ**: Río Negro-Juruena. **RO**: Rondonia-San Ignacio. **S**: Sunsás. **VT**: Ventuari-Tapajos. Pie chart gives the age distribution in percent of the main contributing source provinces.

The three youngest ages between 629 and 552 Ma are from weakly rounded subidiomorphic zircon grains (see Supplementary figure 1). The maximum likelihood age of deposition calculated from the entire sample according to Vermeesch (2021) is 565±18 Ma.

Surprisingly, at Huaitiquina there are no detrital zircon ages reflecting the synsedimentary volcanic activity recorded by the mafic and felsic volcanic rocks intercalated in the Aguada de la Perdiz Formation (see above; Coira and Barber, 1987, 1989; Breitkreuz *et al.,* 1989; Bahlburg, 1990, 1998; Coira *et al.,* 1999, 2009b). The Cryogenian-Ediacaran (Neoproterozoic) maximum likelihood age of deposition (Vermeesch, 2021) of 565±18 Ma derived from the detrital zircon age spectrum is older by *ca*. 100 Myr than the actual Early Ordovician biostratigraphic age of deposition (Fig. 3; Table 1).

The detrital zircon U-Pb age spectrum of the Aguada de la Perdiz Formation at the Huaitiquina location reflects the expected Precambrian Amazonian provenance found in many studies throughout the Andes. In contrast, the absence of synmagmatic Ordovician ages reflecting the syndepositional volcanic activity together with the presence of Cryogenian-Ediacaran youngest ages is an unexpected result. The youngest magmatic event recorded by the data from Huaitiquina is the alleged Olmos magmatic arc in eastern Peru active between 650 and 550 Ma (Chew *et al.,* 2008; Bahlburg *et al.,* 2025) and before the onset of the Pampean orogenic cycle (540-520 Ma; Rapela *et al.,* 1998a,b). However, the few detrital zircon U-Pb ages obtained from the formation at the Aguada de la Perdiz location constrain the age of the sampled layer at 465±4 Ma (lower Darriwilian; n=5; Einhorn *et al.,* 2015). Similar ages are also abundant farther west in the CISL and to the east in the mainly Middle Ordovician Puna Turbidite Complex (Bahlburg and Zimmermann, 2025; Figs. 1 and 7). This indicates

that sediment routing systems from the Famatinian magmatic arc in fact delivered Famatinian detritus to the considered formations. They appear, however, to have bypassed the Huaitquina locality.

Detrital zircon age spectra of the Ediacaran-Early Cambrian siliciclastic Puncoviscana Formation involved in the formation of the Pampean orogenic cycle in northwestern Argentina (Ramacciotti *et al.,* 2025) show age distributions similar to the Huaitiquina sample. The detritus recorded in sample HY19 could therefore have been derived from reworking of the Puncoviscana rocks. However, both the position of the Aguada de la Perdiz Formation on the eastern flank of the Famatinian magmatic arc and the east-directed paleocurrent and eastward deepening facies trends of the Ordovician basin in the Puna of Argentina make a provenance from the Puncoviscana formation from eastern side of the basin unlikely.

The coeval magmatism of the Faja Eruptiva de la Puna Oriental in the eastern Puna and east of the Puna Volcanic Complex (Coira *et al.,* 1999; Bahlburg *et al.,* 2016; Pankhurst *et al.,* 2016) (Fig. 1) is also not registered at the Huaitiquina locality. This is probably due to the deeper Early Ordovician basin between this magmatic zone and the Aguada de la Perdiz Formation which may have captured the syndepositional magmatic detritus derived from the east (Bahlburg, 1990).

The data also indicate that the youngest detritus included in the Lower Ordovician siliciclastic deposits at Huaitiquina predominantly reflects a potentially polycyclic derivation from sources older by 100 to 200 Myr, having bypassed Pampean sources of 540-520 Ma (Rapela *et al.,* 1998a, b).

6. Discussion and Conclusions

The Puna Volcanic Complex is separated into two parts by the diachronous angular Tumbaya unconformity (Moya, 2015) (Fig. 3). Units below this unconformity include the Las Vicuñas Formation north of the Salar del Rincón (Moya *et al.,* 1993) and the CISL in northern Chile (Niemeyer, 1989) (Fig. 1), both belonging to the Tremadocian (Fig. 3). The Aguada de la Perdiz Formation was deposited above the unconformity, with an upper Floian to lower Darriwilian age. At the type locality this biostratigraphic age coincides with very scarce detrital zircon age data between 475 and 465 Ma.

The Quebrada Grande Formation in the Cordón de Lila in northern Chile overlies the CISL unconformity and has a Darriwilian biostratigraphic age based on brachiopods and graptolites (González *et al.,* 2007) (Fig. 1; Table 1). However, the CISL and the Quebrada Grande and Aguada de la Perdiz formations have very similar depositional ages as defined by U-Pb zircon age data. The youngest age cluster obtained from the CISL turbidites yielded a weighted mean age of 477±5 Ma with a youngest zircon age of 475±11 Ma (Augustsson *et al.,* 2015). Rhyolite and dacite lava intercalations gave ages between 480 and 470 Ma (Zimmermann *et al.,* 2010; Pankhurst *et al.,* 2016). Coeval intrusive activity is recorded in the Cordón de Lila between 485 and 471 Ma (Pankhurst *et al.,* 2016) (Fig. 1). The Quebrada Grande Formation equally includes rhyolite and dacite lava flows dated at *ca.* 480, 477 and 470 Ma in its lower part (Zimmermann *et al.,* 2010; Pankhurst *et al.,* 2016) (Fig. 3). Pampean detrital zircon ages are scarce here as well but those reflecting the Olmos magmatic arc between 650 and 550 Ma are abundant with a peak age at *ca*. 640 Ma (Augustsson *et al.,* 2015). Considering both the biostratigraphic and detrital zircon U-Pb ages of the Aguada de la Perdiz Formation, the CISL and the Quebrada Grande Formation, the differences between all three formations in physical stratigraphy and biostratigraphy can presently not be reproduced or resolved by the available geochronological data.

The depositional environment accommodating the variable lithologies of the Aguada de la Perdiz Formation can best be described as a volcaniclastic apron which formed on the eastern flank of the Famatinian magmatic arc which in this region is also named Faja Eruptiva de la Puna Occidental (Palma *et al.,* 1986; Bahlburg, 1990; Coira *et al.,* 2009b).

The sandstones and greywackes of all formations constituting the Puna Volcanic Complex are predominantly compositionally immature and uniformly rich in feldspar and rock fragments. They have a rhyodacitic to rhyolitic upper crustal geochemical composition similar to magmatic arcs (Bahlburg, 1998; Zimmermann and Bahlburg, 2003; Zimmermann *et al.,* 2010; Zimmermann, unpublished data on the Las Vicuñas Formation).

There are notable differences between the detrital zircon U-Pb age spectra of the CISL and the Aguada de la Perdiz Formation at the Huaitiquina locality. The distribution of ages and their abundances in

samples of both formations reflect an expected Precambrian Amazonian provenance previously also obtained in many sandstone studies throughout the Andes (*e.g.,* Willner *et al.,* 2008; Bahlburg *et al.,* 2009, 2011, 2025; Augustsson *et al.,* 2015; Einhorn *et al.,* 2015; Pankhurst *et al.,* 2016). An unexpected result is the absence of synmagmatic Ordovician ages and the presence of Ediacaran youngest ages in the Huaitiquina sample (Figs. 3 and 7). The youngest magmatic event recorded by the Huaitiquina data is the inferred Olmos magmatic arc in eastern Peru active between 650 and 550 Ma (Chew *et al.,* 2008; Bahlburg *et al.,* 2025) and before the onset of the Pampean orogenic cycle (Rapela *et al.,* 1998a, b). Famatinian zircons are present at the Aguada de la Perdiz type locality (Einhorn *et al.,* 2015) but absent from the Huaitquina locality where Olmos-Pampean ages form the youngest age population (Fig. 7). The variable age distributions indicate that erosion in the region of the Famatinian arc source supplied detritus unevenly to the various depositional sites and that it had locally dissected the volcanic edifices to progressively access the arc basement.

Acknowledgements

We are indebted to Professor F. Hervé for his friendship and cooperation in many projects. Extended amicable discussions of the geology of the Andes over almost 40 years were spent sharing many a Pisco Sour and Chilean wine. We commend J. Maletz, Berlin, for his exhaustive reconsideration of pertinent graptolite data. The analysis of detrital zircon U-Pb ages was facilitated by J. Berndt and B. Schmitte at Institut für Mineralogie, Universität Münster, and was made possible by grant BA 1011/45-1 of the German Research Foundation (DFG) to HB. We appreciate the constructive reviews by C. Cisterna, L. Pinto and C. Ramacciotti, and the editorial guidance by R. Pankhurst and D. Bertin.

References

Aceñolaza, F.G.; Durand, F.R. 1975. Contribución al conocimiento bioestratigráfico del Ordovícico puneño, fauna graptolítica de Catúa, provincias de Salta y Jujuy. *In* Congreso Argentino de Paleontología y Bioestratigrafía, No. 1, Actas 1: 77-89. Tucumán.

Aceñolaza, F.G.; Baldis, B. 1987. The Ordovician system of South America. Correlation chart and explanatory notes. International Union of Geological Sciences Publication 22: 68 p.

Alasino, P.H.; Larrovere, M.A.; Ratschbacher, B.C.; Casquet, C.; Paterson, S.R. 2024. Famatinian magmatism in the SW Gondwana margin: A review focused on the Sierras Pampeanas (Argentina). Journal of South American Earth Sciences 145: 105035. https://doi.org./10.1016/j.jsames.2024.105035

Armas, P.; Cristofolini, E.A.; Otamendi, J.E.; Tibaldi, A.M.; Barzola, M.G.; Camilletti, G.C. 2018. Geochronology and facies analysis of subaqueous volcanism of lower ordovician, Famatinian arc, Argentina. Journal of South American Earth Sciences 84: 255-265. https://doi.org/10.1016/j.jsames.2018.04.005

Armas, P.; Cristofolini, E.; Escribano, F.; Camilletti, G.; Barzola, M.; Otamendi, J.; Cisterna, C.; Leisen, M.; Romero, R.; Barra, F.; Tibaldi, A. 2021. Lower-middle Ordovician sedimentary environment and provenance of the Suri formation in the northern region of the Famatina belt, Catamarca, Argentina. Journal of South American Earth Sciences 105: 102948. https://doi.10.1016/j.jsames.2020.102948

Augustsson, C.; Rüsing, T.; Niemeyer, H.; Kooijman, E.; Berndt, J.; Bahlburg, H.; Zimmermann, U. 2015. 0.3 b.y. of drainage stability along the Palaeozoic palaeo-Pacific Gondwana margin - a detrital zircon study. Journal of the Geological Society, London, 172: 186-200. https://doi.org/10.1144/jgs2014-065

Bahlburg, H. 1990. The Ordovician basin in the Puna of NW Argentina and N Chile: geodynamic evolution from back-arc to foreland basin. Geotektonische Forschungen 75: 1-107.

Bahlburg, H. 1998. The geochemistry and provenance of Ordovician turbidites in the Argentinian Puna. *In* The Proto-Andean Margin of Gondwana (Pankhurst, R.J.; Rapela, C.W.; editors). Geological Society, London, Special Publication 142: 127-142. London. http://dx.doi.org/10.1144/gsl.sp.1998.142.01.07

Bahlburg, H.; Zimmermann, U. 2025. Multi-sample detrital zircon provenance variations within a single turbidite complex – The Ordovician Puna Turbidite Complex in the Puna retroarc foreland basin of northwestern Argentina. Geological Magazine 162: 1-15. https://doi.org/10.1017/S0016756825100423

Bahlburg, H.; Breitkreuz, C.; Maletz, J.; Moya, M.C.; Salfity, J.A. 1990. The Ordovician sedimentary rocks in the northern Puna of Argentina and Chile: New stratigraphical data based on graptolites. Newsletters on Stratigraphy 23: 69-89. https://doi.org/10.1127/nos/23/1990/69

Bahlburg, H.; Carlotto, V.; Cárdenas, J. 2006. Evidence of Early to Middle Ordovician arc volcanism in the

Cordillera Oriental and Altiplano of southern Peru, Ollantaytambo Formation and Umachiri beds. Journal of South American Earth Sciences 22 (1-2): 52-65. https://doi.org/10.1016/j.jsames.2006.09.001

Bahlburg, H.; Vervoort, J.D.; Du Frane, S.A.; Bock, B.; Augustsson, C. 2009. Timing of accretion and crustal recycling at accretionary orogens: Insights learned from the western margin of South America. Earth-Science Reviews 97: 227-253.

Bahlburg, H.; Vervoort, J.D.; DuFrane, A.; Carlotto, V.; Reimann, C.; Cárdenas, J. 2011. The U-Pb and Hf isotope evidence of detrital zircons of the Ordovician Ollantaytambo Formation, southern Peru, and the Ordovician provenance and paleogeography of southern Peru and northern Bolivia. Journal of South American Earth Sciences 32: 196-209. https://doi.org/10.1016/j.jsames.2011.07.002

Bahlburg, H.; Berndt, J.; Gerdes, A. 2016. The ages and tectonic setting of the Faja Eruptiva de la Puna Oriental, Ordovician, NW Argentina. Lithos 256-257: 41-54. https://doi.org/10.1016/j.lithos.2016.03.018

Bahlburg, H.; Zimmermann, U.; Matos, R.; Berndt, J.; Jiménez, N.; Gerdes, A. 2020. The missing link of Rodinia break up in western South America: A petrographical, geochemical, and zircon Pb-Hf isotope study of the volcanosedimentary Chilla beds (Altiplano, Bolivia). Geosphere 16: 619-645. https://doi.org/10.1130/GES02151.1

Bahlburg, H.; Kemp, A.I.S.; Fanning, C.M.; Martin, L. 2025. The Hf and O isotope record of long-lasting accretionary orogens: The example of the Proterozoic and Paleozoic-Triassic central South America. Earth-Science Reviews 262: 105068. https://doi.org/10.1016/j.earscirev.2025.105068

Benedetto, J.L. 2001. Una fauna de braquiópodos arenigianos (Ordovícico temprano) en rocas volcanoclásticas de la Puna occidental de Argentina: implicaciones paleoclimáticas y paleogeográficas. Ameghiniana 38: 131-146.

Benedetto, J.L. 2003. The Ordovician brachiopod faunas of Argentina. *In* Ordovician fossils of Argentina. Secretaria de Ciencia y Tecnología (Benedetto, J.L.; editor). Universidad Nacional de Córdoba: 21 p.

Benedetto, J.L.; Niemeyer, H.; González, J.; Brussa, E.D. 2008. Primer registro de braquiópodos y graptolitos ordovícicos en el Cordón de Lila (Puna de Atacama), norte de Chile. Ameghiniana 45 (1): 3-12.

Breitkreuz, C. 1986. Das Paläozoikum in den Kordilleren Nordchiles (21°-25° S). Geotektonische Forschungen 70: 1-88.

Breitkreuz, C.; Bahlburg, H.; Delakowitz, B.; Pichowiak, S. 1989. Paleozoic volcanic events in the Central Andes. Journal of South American Earth Sciences 2 (2): 171-189. https://doi.org/10.1016/0895-9811(89)90045-X

Brussa, E.D.; Toro, B.A.; Vaccari, N.E. 2008. Bioestratigrafía del Paleozoico Inferior en el ámbito de la Puna. *In* Geología y recursos naturales de la Província de Jujuy (Coira, B.; Zappettini, E.O.; editors). Relatorio del Congreso Geológico Argentino, No. 17: 93-97. Jujuy

Cas, R.; Wright, J.V. 1987. Volcanic successions: modern and ancient. Allen & Unwin: 1-528. London.

Cawood, P.A. 2005. Terra Australis Orogen: Rodinia breakup and development of the Pacific and Iapetus margins of Gondwana during the Neoproterozoic and Paleozoic. Earth-Science Reviews 69 (3): 249-279. https://doi.org/10.1016/j.earscirev.2004.09.001

Cawood, P.A.; Strachan, R.A.; Pisarevsky, S.A.; Gladkochub, D.P.; Murphy, J.B. 2016. Linking collisional and accretionary orogens during Rodinia assembly and breakup: Implications for models of supercontinent cycles. Earth and Planettary Science Letters 449: 118-126. https://doi.org/10.1016/j.epsl.2016.05.049

Chew, D.M.; Magna, T.; Kirkland, C.L.; Mišković, A.; Cardona, A.; Spikings, R.A.; Schaltegger, U. 2008. Detrital zircon fingerprint of the Proto-Andes: Evidence for a Neoproterozoic active margin? Precambrian Research 167: 186-200. https://doi.org/10.1016/j.precamres.2008.08.002

Cisterna, C.E.; Coira, B. 2022. Ordovician submarine to subaerial volcanism along the western Gondwana margin: records of the Famatinian belt evolution, northwestern Sierras Pampeanas, Argentina. International Journal of Earth Sciences111: 675-701. https://doi.org/10.1007/s00531-021-02141-6

Cohen, K.M.; Finney, S.C.; Gibbard, P.L. Fan, J.-X. 2013. updated. The ICS International Chronostratigraphic Chart. Episodes 36 (3): 199-204. https://doi.org/10.18814/epiiugs/2013/v36i3/002

Coira, B.; Barber, E. 1987. Vulcanismo submarino Ordovícico (Arenigiano-Llanvirniano) del Río Huaitiquina, Provincia de Salta, Argentina. *In* Congreso Geológico Argentino, No. 10, Actas 4: 305-307. San Miguel de Tucumán.

Coira, B.; Barber, E. 1989. Vulcanismo submarino Ordovícico (Arenigiano-Llanvirniano) del Río Huaitiquina, Provincia de Salta, Argentina. Revista de la Asociación Geológica Argentina 44: 68-77.

Coira, B.; Nullo, F. 1989. Facies piroclásticas del vulcanismo Ordovícico (Arenigiano-Llanvirniano), Salina de Jama, Jujuy. Revista de la Asociación Geológica Argentina 44: 89-95.

Coira, B.; Davidson, J.; Mpodozis, C.; Ramos, V. 1982. Tectonic and magmatic evolution of the Andes of northern Argentina and Chile. Earth-Science Reviews 18: 303-332.

Coira, B.; Koukharsky, M.; Pérez, A. 1987. Rocas volcaniclásticas ordovícicas de la Sierra de Guayaos, Provincia de Salta, Argentina. *In* Congreso Geológico Argentino, No. 10, Actas 4: 312-315. San Miguel de Tucumán.

Coira, B.; Kay, S.M.; Peréz, B.; Woll, B.; Hanning, M.; Flores, P. 1999. Magmatic Sources and tectonic Setting of Gondwana Ordovician Magmas, Northern Puna of Argentina and Chile. *In* Laurentia-Gondwana connections before Pangaea (Ramos, V.A.; Keppie, J.D.; editors). Geological Society of America Special Paper 336: 145-170. Boulder.

Coira, B.; Kirschbaum, A.; Hongn, F.; Pérez, B.; Menegatti, N. 2009a. Basic magmatism in northeastern Puna, Argentina: Chemical composition and tectonic setting in the Ordovician back-arc. Journal of South American Earth Sciences 28 (4): 374-382. https://doi.org/10.1016/j.jsames.2009.04.007

Coira, B.; Koukharsky, M.; Ribeiro Guevara, S.; Cisterna, C.E. 2009b. Puna (Argentina) and northern Chile Ordovician basic magmatism-A contribution to the tectonic setting. Journal of South American Earth Sciences 27 (1): 24-35. https://doi.org/10.1016/j.jsames.2008.10.002

Cordani, U.G.; Teixeira, W. 2007. Proterozoic accretionary belts in the Amazonian Craton. *In* 4-D Framework of Continental Crust. (Hatcher, R.D., Jr.; Carlson, M.P.; McBride, J.H.; Martínez Catalán, J.R.; editors). Geological Society of America Memoir 200: 297-320. https://doi.org/10.1130/2007.1200(14)

Einhorn, J.C.; Gehrels, G.E.; Vernon, A.; DeCelles, P.G. 2015. U-Pb zircon geochronology of Neoproterozoic-Paleozoic sandstones and Paleozoic plutonic rocks in the Central Andes (21°S-26°S). *In* Geodynamics of a Cordilleran Orogenic System: The Central Andes of Argentina and Northern Chile. (DeCelles, P.G.; Ducea, M.N.; Carrapa, B.; Kapp, P.A.; editors). Geological Society of America Memoir 212: 115-124. https://doi.org/10.1130/2015.1212(06)

Fuenzalida, H. 1957. Pizarras y cuarcitas de la localidad de Mucar. *In* Léxique Stratigraphique International (Hoffstetter, R.; Fuenzalida, H.; Cecioni, G.; editors), Centre National de la Recherche Scientifique, Vol. V, Amérique Latin, Fascule 7, "Chile". Chili...: 444 p.

García, A.F.; Perez D'Angelo, E.; Ceballos, S.E. 1962. El Ordovícico de Aguada de la Perdiz, Puna de Atacama, provincia de Antofagasta. Revista Mineralógica 77: 52-61.Santiago.

Goldman, D.; Leslie, S.A.; Liang, Y.; Bergström, S.M. 2023. Ordovician biostratigraphy: index fossils, biozones and correlation. Geological Society, London, Special Publications 532: 31-62. London. https://doi.org/10.1144/SP532-2022-49

González, J.; Niemeyer, H.; Benedetto, J.L.; Brussa, E.D. 2007. The Ordovician Quebrada Grande Formation, Cordón de Lila (Antofagasta Region, northern Chile): stratigraphic and palaeogeographic significance. Revista Geológica de Chile 34 (2): 277-290.

Gutiérrez-Marco, J.C.; Aceñolaza, G.F.; Esteban, S.B. 1996. Revisión de algunas localidades con graptolitos ordovícicos en la Puna salto-jujeña (noroeste de Argentina). *In* Congreso Geológico de Bolivia (Tarija), No. 12, Memorias 2: 725-731. Tarija.

Haeberlin, Y.; Fontboté, L. 2002. The Eastern Cordillera of northern Peru, the remains of a lower Paleozoic collisional belt: new evidence from the Pataz region (7°40'-8°10'S). *In* Geological and structural setting, age, and geochemistry of the orogenic gold deposits at the Pataz Province, Eastern Andean Cordillera, Peru (Haeberlin, Y.; editor). Terre and Environnement 36: 21-48.

Kooijman, E.; Berndt, J.; Mezger, K. 2012. U-Pb dating of zircon by laser ablation ICP-MS: Recent improvements and new insights. European Journal of Mineralogy 24 (1): 5-21. https://doi.org/10.1127/0935-1221/2012/0024-2170

Marinovic, N. 1979. Geología de los cuadrángulos Zapaleri y Nevados de Poquis, II Región Chile. Memoria de Título (Unpublished), Universidad de Chile, Departamento de Geología: 75 p.

Méndez, V.; Turner, J.C.M.; Navarini, A.; Amengual, R.; Viera, V. 1979. Geología de la región noroeste, Provincias Salta y Jujuy, República Argentina. Dirección General de Fabricaciones Militares: 118 p. Buenos Aires.

Monteros, J.A.; Moya, M.C.; Monaldi, C.R. 1996. Graptofaunas arenigianas en el borde occidental de La Puna argentina. lmplicancias paleogeográficas. *In* Congreso Geológico de Bolivia, No. 12, Memorias 2: 733-746. Tarija.

Moya, M.C. 2015. La "Fase Oclóyica" (Ordovícico Superior) en el noroeste argentino. Interpretación histórica y evidencias en contrario. Serie Correlación Geológica 31: 73-110. San Miguel de Tucumán.

Moya, M.C.; Malanca, S.; Hongn, F.D.; Bahlburg, H. 1993. El Tremadoc temprano en la Puna occidental argentina. *In* Congreso Geológico Argentino, No. 12, Actas 2: 20-30. Mendoza.

Niemeyer, H. 1989. El complejo ígneo-sedimentario del Cordón de Lila, región de Antofagasta: Significado tectónico. Revista Geológica de Chile 16 (2): 163-181.

Niemeyer, H.; Götze, J.; Sanhueza, M.; Portilla, C. 2018. The Ordovician magmatic arc in the northern Chile-Argentina Andes between 21° and 26° south latitude. Journal of South American Earth Sciences 81: 204-214. https://doi.org/10.1016/j.jsames.2017.11.016

Otamendi, J.E.; Tibaldi, A.M.; Vujovich, G.I.; Vinao, G. 2008. Metamorphic evolution of migmatites from the deep Famatinian arc crust exposed in sierras Valle Fertil-La Huerta, San Juan, Argentina. Journal of South American Earth Sciences 25: 313-335.

Palma, M.A.; Parica, P.D.; Ramos, V.A. 1986. El granito de Archibarca: Su edad y significado tectónico, provincia de Catamarca. Revista de la Asociación Geológica Argentina 41 (3): 414-419.

Pankhurst, R.J.; Rapela, C.W.; Saavedra, J.; Baldo, E.; Dahlquist, J.; Pascua, I.; Fanning, C.M. 1998. The Famatinian magmatic arc in the central Sierras Pampeanas: an Early to Mid-Ordovician continental arc on the Gondwana margin. *In* The Proto-Andean Margin of Gondwana (Pankhurst, R.J.; Rapela, C.W.; editors). The Geological Society of London, Special Publication 142 (1): 343-367.

Pankhurst, R.J.; Hervé, F.; Fanning, M.C.; Calderón, M.; Niemeyer, H.; Griem-Klee, S.; Soto, F. 2016. The pre-Mesozoic rocks of northern Chile: U-Pb ages, and Hf and O isotopes. Earth-Science Reviews 152: 88-105. https://doi.org/10.1016/j.earscirev.2015.11.009

Pepper, M.; Gehrels, G.; Pullen, A.; Ibánez-Mejía, M.; Ward, K.M.; Kapp, P. 2016. Magmatic history and crustal genesis of western South America: Constraints from U-Pb ages and Hf isotopes of detrital zircons in modern rivers. Geosphere 12 (5): 1532-1555. https://doi.org/10.1130/GES01315.1

Pérez, E. 1983. Estado actual del conocimiento del Cambro Ordovícico en Chile. *In* Programa Internacional de Correlación Geológica, Proyecto 192. Desarrollo del Cámbrico y Ordovícico de Latinoamérica. Reunión del grupo de Trabajo Internacional, No. 2. Correlación Geológica, No. 1: 88-98. Cartagena de Indias.

Pérez, E.; Davidson, J. 1982. Turbiditas ordovícicas en la Puna de Antofagasta, Chile: consideraciones paleogeográficas. *In* Congreso Geológico Chileno, No. 3, Resúmenes: 21-22. Concepción.

Ramacciotti, C.D.; Larrovere, M.A.; Casquet, C.; Lembo Wuest, C.I.; Morales Cámera, M.M.; Alasino, P.H.; Murra, J.A.; Riveros, A.; Basei, M.A.S.; Herazo, L.; Baldo, E.G. 2025. The Ediacaran margin of the Proterozoic MARA block and the sedimentary basins of the Clymene Ocean: Insights from U-Pb zircon geochronology in the Puna-Sierras Pampeanas transition, NW Argentina. Precambrian Research 422: 107792.

Ramos, V.A. 2018. The Famatinian orogen along the protomargin of Western Gondwana: Evidence for a nearly continuous Ordovician magmatic arc between Venezuela and Argentina. *In* The Evolution of the Chilean-Argentinian Andes (Folguera, A.;Contreras-Reyes, E.; Heredia, N.;Encinas, A.; Iannelli, S.B; Oliveros, V.; Dávila, F.M.; Collo, G.; Giambiagi, L.; Maksymowicz, A.; Iglesia Llanos, M.P.; Turienzo, M.; Naipauer, N.; Orts, D.; Litvak, V.D.; Álvarez O.; Arriagada, C.; editors) Springer Earth System Sciences: 154-183.

Rapela, C.W.; Toselli, A.; Heaman, L.; Saavedra, J. 1990. Granite plutonism in the Sierras Pampeanas; an inner cordilleran Paleozoic arc in the southern Andes. *In* Plutonism from Antarctica to Alaska (Mahlburg Kay, S.; Rapela, C.W.; editors). Geological Society of America Special Paper 241: 77-90.

Rapela, C.W.; Pankhurst, R.J.; Casquet, C.; Baldo, E.; Saavedra, J.; Galindo, C.; Fanning, C.M. 1998a. The Pampean Orogeny of the southern proto-Andes: Cambrian continental collision in the Sierras de Córdoba. *In* The Proto-Andean Margin of Gondwana (Pankhurst, R.J.; Rapela, C.W.; editors). Geological Society, London, Special Publication 142 (1): 181-217. https://doi.org/10.1144/GSL.SP.1998.142.01.10

Rapela, C.W.; Pankhurst, R.J.; Casquet, C.; Baldo, E.; Saavedra, J.; Galindo, C. 1998b. Early evolution of the Proto-Andean margin of South America. Geology 26 (8): 707-710. https://doi.org/10.1130/0091-7613(1998)026<0707:EEOTPA>2.3.CO;2

Rapela, C.W.; Pankhurst, R.J.; Casquet, C.; Dahlquist, J.A.; Fanning, C.M.; Baldo, E.G.; Galindo, C.; Alasino, P.H.; Ramacciotti, C.D.; Verdecchia, S.O.; Murra, J.A.; Basei, M.A.S. 2018. A review of the Famatinian Ordovician magmatism in southern South America: evidence of lithsophere reworking and continental subduction in the early proto-Andean margin of Gondwana. Earth-Science Reviews 187: 259-285.

Schwab, K. 1973. Die Stratigraphie in der Umgebung des Salar de Cauchari (NW Argentinien). Ein Beitrag zur erdgeschichtlichen Entwicklung der Puna. Geotektonische Forschungen 43: 1-168.

Spencer, C.J.; Kirkland, C.L.; Taylor, R.J.M. 2016. Strategies towards statistically robust interpretations of *in situ* U-Pb zircon geochronology. Geoscience

Frontiers 7 (4): 581-589. https://doi.org/10.1016/j.gsf.2015.11.006

Toro, B.A.; Herrera Sánchez, N.C. 2019. Stratigraphical distribution of the Ordovician graptolite *Azygograptus* Nicholson & Lapworth in the Central Andean Basin (northwestern Argentina and southern Bolivia). Comptes Rendus Palevol 18 (5): 493-507. https://doi.org/10.1016/j.crpv.2019.06.002

Toro, B.A.; Heredia, S.; Herrera Sánchez, N.C.; Moreno, F.; Lo Valvo, G. 2019. First conodonts record in the Argentine Puna related to Middle Ordovician graptolites. Publicación Electrónica de la Asociación Paleontológica Argentina 19: R82-R83.

Toro, B.A.; Heredia, S.; Herrera Sánchez, N.C.; Moreno, F. 2020. First Middle Ordovician conodont record related to key graptolites from the western Puna, Argentina: Perspectives for an integrated biostratigraphy and correlation of the Central Andean Basin. Andean Geology 47: 144-161. http://dx.doi.org/10.5027/andgeoV47n1-3261

Vavra, G.; Schmid, R.; Gebauer, D. 1999. Internal morphology, habit and U-Th-Pb microanalysis of amphibolite-to-granulite facies zircons: geochronology of the Ivrea Zone (Southern Alps). Contributions to Mineralogy and Petrology 134: 380-404.

Vermeesch, P. 2021. Maximum depositional age estimation revisited. Geoscience Frontiers 12: 843-850. https://doi.org/10.1016/j.gsf.2020.08.008

Vermeesch, P.; Resentini, A.; Garzanti, E. 2016. An R package for statistical provenance analysis. Sedimentary Geology 336: 14-25. https://doi.org/10.1016/j.sedgeo.2016.01.009

Weinberg, R.F.; Becchio, R.; Farías, P.; Suzaño, N.; Sola, A. 2018. Early Paleozoic accretionary orogenies in NW Argentina: Growth of West Gondwana. Earth-Science Reviews 187: 219-247. https://doi.org/10.1016/j.earscirev.2018.10.001

White, J.D.L.; Busby-Spera, C. 1987. Deep marine arc apron deposits and syndepositional magmatism in the Alisitos Group at Punta Cono, Baja California, Mexico. Sedimentology 34: 911-927. https://doi.org/10.1111/J.1365-3091.1987.TB00812.X

Willner, A.; Lottner, U.; Miller, H. 1987. Early Paleozoic structural development in the NW Argentine basement of the Andes and its implications for geodynamic reconstructions. *In* Gondwana six: Structure, tectonics and geophysics (McKenzie, G.D.; editor). American Geophysical Union Monograph 40: 229-239. https://doi.org/10.1029/GM040p0229

Willner, A.P.; Gerdes, A.; Masonne, H.J. 2008. History of crustal growth and recycling at the Pacific convergent margin of South America at latitudes 29°-36° S revealed by a U-Pb and Lu-Hf isotope study of detrital zircon from late Paleozoic accretionary systems. Chemical Geology 253: 114-129. https://doi.org/10.1016/j.chemgeo.2008.04.016

Zimmermann, U.; Bahlburg, H. 2003. Provenance analysis and tectonic setting of the Ordovician deposits in the southern Puna basin, NW Argentina. Sedimentology 50: 1079-1104. https://doi.org/10.1046/j.1365-3091.2003.00595.x

Zimmermann, U.; Niemeyer, H.; Meffre, S. 2010. Revealing the continental margin of Gondwana: the Ordovician arc of the Cordón de Lila (northern Chile). International Journal of Earth Sciences 99 (Suppl 1): S39-S56. https://doi.org/10.1007/s00531-009-0483-8

Manuscript received: May 22, 2025; revised/accepted: September 11, 2025; available online: September 11, 2025.

Supplementary material

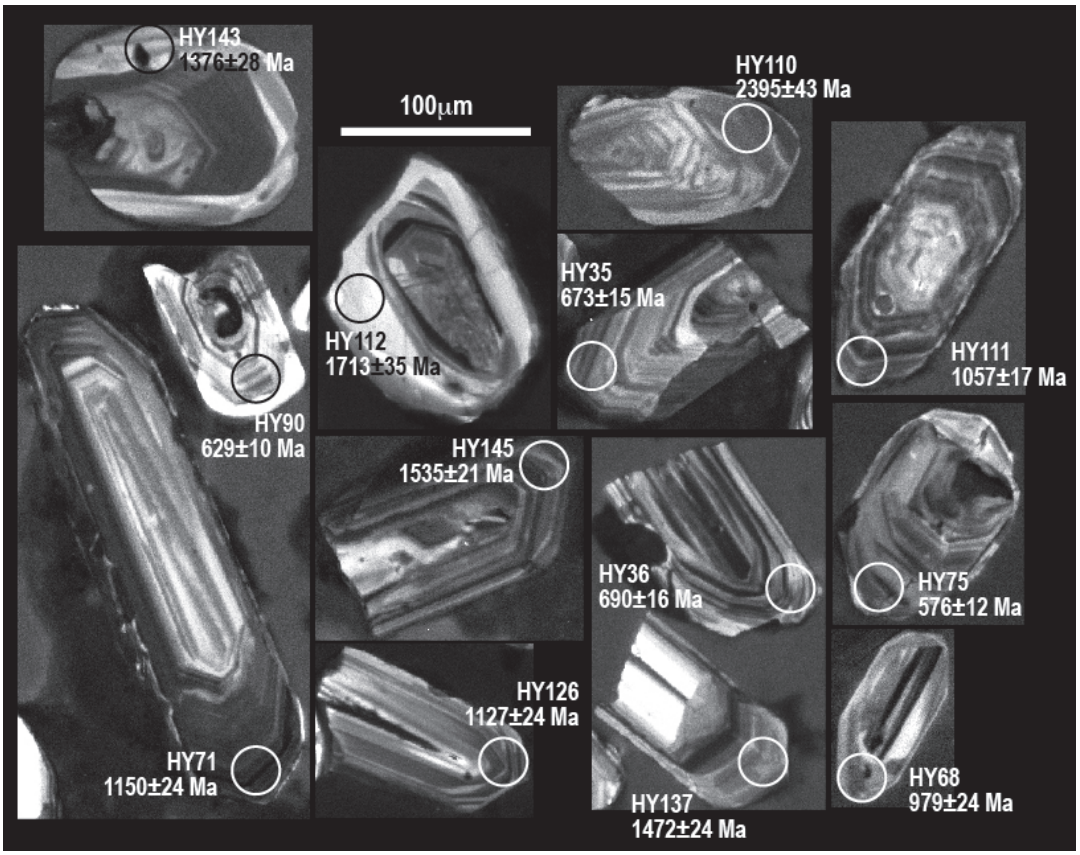

SUPPLEMENTARY FIGURE 1. Representative cathodoluminescence (CL) images of zircons predominantly showing oscillatory zoning characteristic of a magmatic origin. The circles indicate the positions of 25 mm diameter U-Pb isotope laser ablation spots.

SUPPLEMENTARY TABLE 1. DETRITAL ZIRCON AGE DATA OF SAMPLE HY19.

Sample name	$^{238}U/^{206}Pb$	2σ (%)	$^{207}Pb/^{206}Pb$	2σ (%)	$^{206}Pb/^{238}U$ (age)	2σ (age)	$^{207}Pb/^{206}Pb$ (age)	2σ (age)	discordance
HY19_147	11.1874	1.73%	0.0585	4.62%	551.9	9.2	548.9	101.0	-0.5%
HY19_75	10.7032	2.22%	0.0597	3.70%	575.8	12.2	592.6	80.2	2.8%
HY19_90	9.7634	1.58%	0.0615	5.09%	628.6	9.5	657.6	109.4	4.4%
HY19_125	9.4074	2.22%	0.0629	5.48%	651.2	13.8	705.6	116.9	7.7%
HY19_136	9.3774	2.49%	0.0615	3.62%	653.2	15.4	655.2	77.7	0.3%
HY19_35	9.0833	2.37%	0.0619	2.70%	673.3	15.2	671.8	57.9	-0.2%
HY19_36	8.8553	2.37%	0.0634	2.89%	689.7	15.5	722.1	61.4	4.5%
HY19_94	6.7219	3.41%	0.0697	4.93%	894.0	28.5	919.8	101.5	2.8%
HY19_130	6.5625	2.52%	0.0700	3.58%	914.3	21.5	927.5	73.6	1.4%
HY19_18	6.3827	4.07%	0.0703	3.09%	938.2	35.6	938.5	63.3	0.0%
HY19_51	6.3637	2.20%	0.0722	2.27%	940.8	19.3	990.5	46.2	5.0%
HY19_150	6.3262	1.51%	0.0712	6.62%	946.0	13.2	962.3	135.6	1.7%
HY19_68	6.0993	2.60%	0.0720	4.05%	978.7	23.6	984.9	82.5	0.6%
HY19_63	5.9977	0.86%	0.0725	6.41%	994.0	7.9	1,001.2	130.4	0.7%
HY19_78	5.9818	1.37%	0.0744	17.11%	996.5	12.6	1,052.6	350.4	5.3%
HY19_19	5.9198	3.27%	0.0739	6.00%	1,006.1	30.4	1,038.5	121.5	3.1%
HY19_74	5.8482	2.04%	0.0734	6.77%	1,017.5	19.2	1,025.0	137.4	0.7%
HY19_129	5.7138	1.87%	0.0741	2.95%	1,039.6	18.0	1,044.1	59.5	0.4%
HY19_133	5.6986	1.77%	0.0742	2.50%	1,042.2	17.0	1,048.0	50.4	0.6%
HY19_111	5.6116	1.71%	0.0744	3.19%	1,057.1	16.7	1,051.9	64.2	-0.5%
HY19_82	5.6055	3.00%	0.0748	3.50%	1,058.2	29.3	1,062.5	70.4	0.4%
HY19_55	5.5973	0.90%	0.0755	4.18%	1,059.6	8.8	1,081.7	83.8	2.0%
HY19_58	5.5916	1.45%	0.0749	2.57%	1,060.6	14.1	1,067.0	51.7	0.6%
HY19_117	5.5856	2.22%	0.0748	2.12%	1,061.6	21.8	1,063.8	42.6	0.2%
HY19_59	5.5802	1.43%	0.0759	1.30%	1,062.6	14.0	1,092.2	26.0	2.7%
HY19_62	5.4970	1.43%	0.0755	1.52%	1,077.4	14.2	1,081.7	30.4	0.4%
HY19_91	5.4630	2.05%	0.0755	3.21%	1,083.6	20.5	1,082.0	64.5	-0.1%
HY19_96	5.3921	3.06%	0.0766	7.97%	1,096.7	30.8	1,110.0	159.7	1.2%
HY19_98	5.3805	1.52%	0.0770	3.99%	1,098.9	15.3	1,120.9	79.7	2.0%
HY19_60	5.3718	2.41%	0.0765	6.35%	1,100.5	24.4	1,108.4	127.2	0.7%
HY19_72	5.3588	2.29%	0.0765	1.88%	1,102.9	23.2	1,107.6	37.6	0.4%
HY19_40	5.3527	2.29%	0.0767	2.91%	1,104.1	23.3	1,112.6	58.1	0.8%
HY19_107	5.3428	1.87%	0.0765	5.71%	1,106.0	19.0	1,109.2	114.2	0.3%
HY19_41	5.2663	3.28%	0.0768	2.17%	1,120.7	33.7	1,117.0	43.3	-0.3%
HY19_109	5.2632	1.60%	0.0778	2.66%	1,121.3	16.4	1,141.2	52.8	1.7%
HY19_64	5.2541	1.65%	0.0772	1.81%	1,123.1	17.1	1,126.1	36.0	0.3%
HY19_126	5.2356	2.33%	0.0779	12.57%	1,126.8	24.0	1,145.0	252.0	1.6%
HY19_38	5.1814	3.09%	0.0779	2.78%	1,137.6	32.2	1,144.2	55.2	0.6%
HY19_127	5.1376	2.23%	0.0784	2.36%	1,146.4	23.4	1,156.2	46.8	0.8%
HY19_71	5.1219	2.25%	0.0781	3.89%	1,149.7	23.7	1,150.1	77.4	0.0%
HY19_39	5.0846	3.32%	0.0784	2.35%	1,157.4	35.2	1,156.0	46.6	-0.1%

supplementary table 1 continued.

Sample name	$^{238}U/^{206}Pb$	2σ (%)	$^{207}Pb/^{206}Pb$	2σ (%)	$^{206}Pb/^{238}U$ (age)	2σ (age)	$^{207}Pb/^{206}Pb$ (age)	2σ (age)	discordance
HY19_118	5.0099	1.20%	0.0790	2.62%	1,173.1	12.9	1,171.4	51.8	-0.2%
HY19_58c	5.0001	1.66%	0.0796	3.28%	1,175.3	17.8	1,187.0	64.9	1.0%
HY19_138	4.9727	1.46%	0.0790	8.64%	1,181.2	15.8	1,171.7	171.7	-0.8%
HY19_103	4.9600	1.96%	0.0793	7.53%	1,183.9	21.2	1,180.3	149.4	-0.3%
HY19_76	4.8992	3.53%	0.0798	2.82%	1,197.3	38.6	1,190.9	55.6	-0.5%
HY19_128	4.8092	3.00%	0.0828	3.13%	1,217.8	33.3	1,264.8	61.2	3.7%
HY19_50	4.7800	3.00%	0.0814	3.34%	1,224.5	33.5	1,231.7	65.5	0.6%
HY19_57	4.7443	2.18%	0.0829	3.99%	1,232.9	24.5	1,266.4	78.0	2.6%
HY19_6	4.6609	4.32%	0.0827	4.34%	1,253.0	49.2	1,262.8	84.8	0.8%
HY19_65	4.5218	2.95%	0.0849	2.75%	1,287.9	34.4	1,313.3	53.4	1.9%
HY19_85	4.4588	1.34%	0.0863	1.96%	1,304.4	15.9	1,345.4	37.9	3.1%
HY19_10	4.4076	4.17%	0.0851	3.46%	1,318.1	49.8	1,318.0	67.0	0.0%
HY19_86	4.3564	1.84%	0.0861	3.38%	1,332.1	22.2	1,340.6	65.3	0.6%
HY19_34	4.3409	3.30%	0.0866	1.97%	1,336.4	39.9	1,352.3	38.0	1.2%
HY19_48	4.2691	1.62%	0.0876	3.86%	1,356.6	19.8	1,374.8	74.3	1.3%
HY19_66	4.2191	1.39%	0.0875	1.81%	1,371.1	17.2	1,371.4	34.9	0.0%
HY19_143	4.2041	2.29%	0.0873	2.44%	1,375.5	28.4	1,366.9	46.9	-0.6%
HY19_141	4.1969	1.91%	0.0877	1.76%	1,377.7	23.8	1,376.4	33.9	-0.1%
HY19_73	4.1952	2.66%	0.0879	1.54%	1,378.1	33.1	1,380.8	29.6	0.2%
HY19_4	4.0799	2.65%	0.0897	3.05%	1,413.1	33.6	1,419.5	58.4	0.4%
HY19_21	4.0488	3.38%	0.0903	3.20%	1,422.9	43.1	1,432.2	61.1	0.6%
HY19_87	4.0392	2.04%	0.0921	3.90%	1,425.9	26.1	1,469.3	74.1	3.0%
HY19_12	4.0221	4.02%	0.0903	4.11%	1,431.3	51.6	1,432.0	78.5	0.0%
HY19_5	4.0219	3.97%	0.0902	2.88%	1,431.4	50.9	1,429.4	54.9	-0.1%
HY19_2	4.0162	4.28%	0.0908	3.22%	1,433.2	55.1	1,442.8	61.3	0.7%
HY19_102	3.9895	1.75%	0.0917	3.34%	1,441.8	22.7	1,461.9	63.5	1.4%
HY19_47	3.9875	1.74%	0.0906	2.69%	1,442.5	22.4	1,438.2	51.4	-0.3%
HY19_139	3.9596	1.72%	0.0912	2.32%	1,451.6	22.3	1,450.1	44.1	-0.1%
HY19_30a	3.9480	2.96%	0.0913	3.48%	1,455.4	38.6	1,454.0	66.3	-0.1%
HY19_137	3.8976	1.81%	0.0920	2.18%	1,472.2	23.8	1,467.5	41.4	-0.3%
HY19_25	3.8814	1.40%	0.0930	2.77%	1,477.7	18.5	1,488.4	52.4	0.7%
HY19_97	3.8807	1.55%	0.0920	3.32%	1,477.9	20.4	1,467.5	63.1	-0.7%
HY19_135	3.8753	3.14%	0.0925	1.76%	1,479.8	41.5	1,478.1	33.4	-0.1%
HY19_92	3.8551	1.70%	0.0938	3.22%	1,486.7	22.6	1,503.7	60.9	1.1%
HY19_23	3.8496	3.47%	0.0930	3.26%	1,488.6	46.1	1,487.9	61.8	-0.1%
HY19_27	3.8469	0.80%	0.0946	3.71%	1,489.5	10.6	1,521.1	70.1	2.1%
HY19_140	3.8070	2.10%	0.0939	1.98%	1,503.5	28.1	1,505.5	37.5	0.1%
HY19_145c	3.7971	2.00%	0.0944	1.45%	1,507.0	26.8	1,515.4	27.5	0.6%
HY19_121	3.7285	2.61%	0.0955	3.31%	1,531.6	35.6	1,537.5	62.4	0.4%
HY19_145	3.7188	1.52%	0.0955	2.20%	1,535.2	20.8	1,537.8	41.4	0.2%
HY19_88	3.6972	2.12%	0.0960	3.96%	1,543.2	29.1	1,547.1	74.4	0.3%

supplementary table 1 continued.

Sample name	$^{238}U/^{206}Pb$	2σ (%)	$^{207}Pb/^{206}Pb$	2σ (%)	$^{206}Pb/^{238}U$ (age)	2σ (age)	$^{207}Pb/^{206}Pb$ (age)	2σ (age)	discordance
HY19_100	3.6779	2.93%	0.0961	2.79%	1,550.4	40.4	1,549.2	52.5	-0.1%
HY19_3	3.6531	3.19%	0.0963	3.20%	1,559.7	44.2	1,554.4	60.1	-0.3%
HY19_83	3.6164	3.16%	0.0972	4.24%	1,573.7	44.2	1,571.5	79.5	-0.1%
HY19_42	3.7430	0.89%	0.0974	4.63%	1,526.3	12.1	1,575.0	86.8	3.1%
HY19_14	3.6097	3.33%	0.0975	2.48%	1,576.3	46.5	1,577.2	46.4	0.1%
HY19_149	3.6035	2.14%	0.0976	3.09%	1,578.7	30.0	1,579.4	57.8	0.0%
HY19_144	3.5983	2.12%	0.0980	5.28%	1,580.8	29.7	1,586.9	98.8	0.4%
HY19_9	3.6588	6.36%	0.0979	4.54%	1,557.5	88.0	1,583.7	85.1	1.6%
HY19_11	3.5864	3.84%	0.0979	3.69%	1,585.4	54.0	1,583.9	69.1	-0.1%
HY19_119	3.5576	2.22%	0.0986	3.05%	1,596.8	31.4	1,597.7	56.9	0.1%
HY19_54	3.5012	1.52%	0.0992	1.81%	1,619.5	21.8	1,609.3	33.7	-0.6%
HY19_56	3.5138	1.17%	0.0997	1.87%	1,614.4	16.7	1,618.9	34.8	0.3%
HY19_101	3.4709	1.93%	0.1005	2.06%	1,632.0	27.8	1,633.8	38.2	0.1%
HY19_24	3.5337	1.84%	0.1007	1.99%	1,606.4	26.2	1,636.8	36.9	1.9%
HY19_44	3.4514	2.67%	0.1008	6.52%	1,640.2	38.7	1,638.1	121.3	-0.1%
HY19_37	3.4829	2.68%	0.1012	2.79%	1,627.0	38.6	1,646.8	51.8	1.2%
HY19_30	3.4165	2.86%	0.1017	2.26%	1,654.9	41.7	1,655.0	42.0	0.0%
HY19_49	3.3681	1.57%	0.1026	1.85%	1,675.9	23.2	1,672.6	34.1	-0.2%
HY19_61	3.3938	2.40%	0.1030	6.58%	1,664.7	35.2	1,678.5	121.9	0.8%
HY19_33	3.3435	1.95%	0.1037	1.85%	1,686.7	28.9	1,690.7	34.1	0.2%
HY19_115	3.3556	2.12%	0.1039	2.45%	1,681.4	31.4	1,694.2	45.2	0.8%
HY19_93	3.3275	2.02%	0.1044	4.23%	1,693.9	30.1	1,703.9	77.9	0.6%
HY19_112	3.3228	1.21%	0.1049	1.91%	1,696.0	18.0	1,713.0	35.1	1.0%
HY19_55a	3.2117	1.59%	0.1068	3.20%	1,747.3	24.3	1,746.0	58.7	-0.1%
HY19_45	3.5054	1.08%	0.1082	2.55%	1,617.8	15.5	1,769.0	46.6	8.5%
HY19_67	3.1291	1.57%	0.1096	1.48%	1,787.6	24.5	1,792.3	27.0	0.3%
HY19_99	3.0996	1.54%	0.1100	2.08%	1,802.5	24.2	1,800.2	37.8	-0.1%
HY19_81	3.1583	1.44%	0.1106	1.96%	1,773.2	22.3	1,808.6	35.5	2.0%
HY19_106	3.1571	1.52%	0.1116	2.64%	1,773.7	23.6	1,826.1	47.8	2.9%
HY19_146	3.0468	1.62%	0.1134	2.17%	1,829.7	25.8	1,854.2	39.3	1.3%
HY19_124	2.9583	1.36%	0.1145	1.59%	1,877.1	22.2	1,872.5	28.7	-0.2%
HY19_105	2.8953	1.87%	0.1171	1.82%	1,912.5	30.9	1,913.0	32.7	0.0%
HY19_114	2.7414	1.40%	0.1251	1.79%	2,004.7	24.1	2,030.5	31.8	1.3%
HY19_13	2.6110	3.65%	0.1284	4.06%	2,090.2	65.2	2,076.8	71.6	-0.6%
HY19_22	2.6678	3.11%	0.1306	2.84%	2,052.0	54.7	2,106.1	49.9	2.6%
HY19_104	2.3695	1.75%	0.1433	9.77%	2,269.6	33.5	2,267.8	169.2	-0.1%
HY19_131	2.4140	3.35%	0.1457	9.11%	2,234.3	63.2	2,296.3	157.3	2.7%
HY19_110	2.2365	1.62%	0.1544	2.51%	2,382.4	32.3	2,394.9	42.7	0.5%
HY19_7	1.8847	4.04%	0.1895	6.04%	2,743.8	90.2	2,738.2	99.6	-0.2%
HY19_84	1.9121	1.92%	0.1904	1.44%	2,711.7	42.5	2,745.3	23.7	1.2%
HY19_120	1.5615	2.71%	0.2534	1.69%	3,190.5	68.1	3,206.3	26.6	0.5%
HY19_148	1.4032	1.34%	0.3116	2.01%	3,468.3	36.0	3,528.7	31.0	1.7%